

LUDWIG-MAXIMILIANS-UNIVERSITÄT MÜNCHEN
FAKULTÄT FÜR GEOWISSENSCHAFTEN
DEPARTMENT FÜR GEOGRAPHIE

BACHELORARBEIT

Wissenschaftliche Arbeit zur Erlangung des akademischen Grades
Bachelor of Science

Remote sensing of coastal erosion and thaw slump activities effected by heavy precipitation in West Alaska

Fernerkundung der Auswirkung von Starkniederschlägen auf Erosionsprozesse in Westalaska

Eingereicht: 03.02.2022, München

Verfasser:

Simon Schäffler
Gabriele-Münter-Str. 9
84489 Burghausen
Matrikelnummer: 11706886

Betreuer:

Prof. Dr. Lukas Lehnert
Luisenstraße 37
80333 München

Abstract

The Arctic region's warming is going much faster than in the rest of the world and is causing degradation of permafrost. About a quarter of the Earth's land mass is characterized by frozen organic carbon-rich ground. The release of this carbon as greenhouse gases is a threat to the world's climate.

In this study the dynamics of retrogressive thaw slumps (RTS), which are main permafrost thawing features along the eroding coasts of the Arctic region, were investigated by using MACS airborne stereo ortho imagery of the 2021 Perma-X flight campaign in West Alaska. The attempt was a remote sensing change detection done by using digital terrain models for structure from motion photogrammetry. The developed workflow was applied at two study sites at the coast of the Baldwin Peninsula. At the time of the data acquisition in June and July 2021 the area was facing heavy rainfalls, which are assumed to occur more often and intensely due to climate change. The aim was to use the results of the digital terrain model differences for measuring the rainfall erosion and their impact on RTS activity.

For processing images photogrammetrically and generating digital elevation models PIX4D was used. Image adjustments and the difference calculations were done with QGIS. Unfortunately the created digital terrain models show a lot of large and small scale failures, which were so severe that a successful DTM differencing was not possible. Mass movement and erosion can be seen at some locations in the DTM, but accurate detecting or measuring of RTS dynamics was not possible with the data and the developed workflow. Therefore the influence of the heavy rainfall event of Summer 2021 remains unclear up to this point.

Contents

List of Figures

1. Introduction	7
1.1 Scientific background	7
1.1.1 Permafrost degradation	7
1.1.2 Remote sensing on Arctic permafrost	10
1.1.3 Retrogressive thaw slumps	12
1.1.4 Climate change related increasing of precipitation	14
1.2 Usability of MACS imagery for DEM differencing	16
1.3 Study Sites	17
2. Methods and material	18
2.1 Workflow	18
2.2 MACS airborne data	21
2.3 Data pre-processing	23
2.4 Progressing and point cloud classification	23
2.4 Image co-Registration	26
2.5 DTM differencing	28
3. Results	29
3.1 Overview	29
3.2 Changes at SA South	30
3.3 Errors at SA South	31
3.4 Changes at SA North	34
3.5 Errors at SA North	36
3.6 Processing errors	37
4. Discussion	39
5. Conclusion	40

Eidesstattliche Erklärung

List of Figures

Fig. 1: Distribution of Permafrost in Alaska (Jorgenson et al., 2008)

Fig. 2: Land Cover Classification on the Baldwin Peninsula (Jongejans et al., 2018)

Fig. 3: Sediments washed into the sea close to the study sites at the Baldwin Peninsula at the 3rd of July 2021 (Grosse, 2021)

Fig. 4: Retrogressive thaw slumps at the Baldwin Peninsula. The central slump has an active slump at the right and an already stabilized part at the left. Underneath the plateau the headwall is seen which is more active at the right. Also the active slump floor is steeper and continues in a sediment flow. Further down at the beach the sediments form a debris cone (Strauss, 2016)

Fig. 5 : Structure of a retrogressive thaw slump (Lantuit and Pollard, 2005)

Fig. 6: Precipitation Trend in Alaska (Alaska Center for Climate Assessment & Policy, University of Alaska Fairbanks, funded by the NOAA Climate Program Office, 2022)

Fig. 7: Last decades' mean annual precipitation in Kotzebue on the Baldwin Peninsula (Necsoiu et al., 2013)

Fig. 8: Location of study sites. Background maps are provided by Google (Google Maps, 2022)

Fig. 9: MACS footprints of PermaX 2021 flight campaign (Nitze, 2021)

Fig. 10: Flowchart of the developed workflow

Fig. 11: Image selection for SA North; A) All images of the flight on 3rd of July 2021; B) 104 images covering SA North; C) SA North actual size. Background maps are provided by Google (Google Maps, 2022)

Fig. 12: Structure-from-motion principle (Sweeney, 2016)

Fig. 13: Automatically classified point cloud in PIX4D

Fig. 14: Defective 3D-DSM

Fig. 15: Comparison of Arosics co-registration offset – global and local

Fig. 16: Vertical offset between 28th of June 2021 and 3rd of July at SA North 2021

Fig. 17: DTM differencing at SA South on the hillshade of the 10th of July 2021

Fig. 18: 3D-Detail of DTM SA South of July 10th 2021; A: DTM covered with DTM difference layer; B: DTM covered with ortho mosaic

Fig. 19: DTM failure; A) DTM Profile Line; B) DTM covered with the ortho mosaic of the 10th of July 2021; C) Profile of the DTM of the 3rd of July 2021 (Blue) and the 10th of July 2021 (Red)

Fig. 20: DTM of the 10th of July 2021 covered with the ortho mosaic and DTM difference

Fig. 21: Vertical offset seen in the profile of the southern area of SA North. Blue: 3rd of July 2021, Red: 10th of July 2021

Fig. 22: DTM differencing SA North between the 28th of June 2021 and the 3rd of July 2021 on the hillshade of the 3rd of July 2021

Fig. 23: 3D-Detail of DTM SA South of July 3rd 2021; A: DTM covered with DTM difference layer; B: DTM covered with ortho mosaic

Fig. 24: DTM differencing SA North between the 3rd and the 10th of July

Fig. 25: Profile of the right $\frac{2}{3}$ of the DTMs at SA North of the 28th of June 2021 (Green), 3rd of July 2021 (Blue) and 10th of July 2021 (Red)

Fig. 26: Profile of the left third of the DTMs at SA North of the 28th of June 2021 (Green), 3rd of July 2021 (Blue) and 10th of July 2021 (Red)

Fig. 27: Even DTM of the 3rd of July 2021 (Blue) and tilted DTM of the 10th of July 2021

Fig. 28: DTM difference at an extra SA between 3rd and 10th of July 2021:

Fig. 29: Displaced image parts caused by matching failures

1. Introduction

1.1 Scientific background

1.1.1 Permafrost degradation

Permafrost is defined as ground of any material whose temperature stays below 0°C for at least two continuous years (Van Everdingen, 2005, 55). The global area underlain by permafrost is about $15 \times 10^6 \text{ km}^2$, which is about 15 % of the Northern Hemisphere land surface (Obu, 2021, 4). The near-surface part of the ground, which is called the active layer, is thawing every season. The thickness of the active layer and the thermal regime of the permafrost varies a lot depending on the climate and ground properties (geology, stratigraphy, vegetation). Especially air temperature and snow cover are important factors (Ling and Zhang, 2003, 149). Due to the fact that the global warming rate in the Arctic is about twice the global rate, permafrost is warming and degrading (Biskaborn et al., 2019, 1). This leads to a destabilization of the ground and has major influences on buildings and infrastructure of Arctic settlements. Especially on the coast, a combination of rising sea level, higher waves and permafrost warming leads to greater coastal erosion rates (Shaw et al., 1998, 44). However also roads, railways and pipelines are in danger with decreasing stability of the ground (Ford and Smit, 2004, 390). Geoengineering solutions like cooling the ground with heat pipes at the Trans-Alaska Pipeline System or building houses on pile foundations are being applied as methods of climate change adaptation (Clarke, 2007, 20; Heuer, 1979, 2).

However the greater threat of thawing permafrost on a global scale is the release of the greenhouse gases carbon dioxide and methane. There are about 1455 billion tons of carbon stored in the northern permafrost zone. The calculation of the actual flux of carbon is difficult, but latest studies estimate about 300-600 million tons of net carbon emissions per year (Schuur, 2019, 58ff).

Jorgenson et al. (2008) describe Alaska's permafrost distribution: "The permafrost zones underlie 80% of Alaska, including continuous (32%), discontinuous (31%), sporadic (8%),

and isolated (10%) permafrost. Glaciers and ice sheets occupy 4% of the area.” Fig. 1 shows the spatial distribution of the zones in Alaska and the depth at several locations. Both study sites are still characterized by continuous permafrost according to this map.

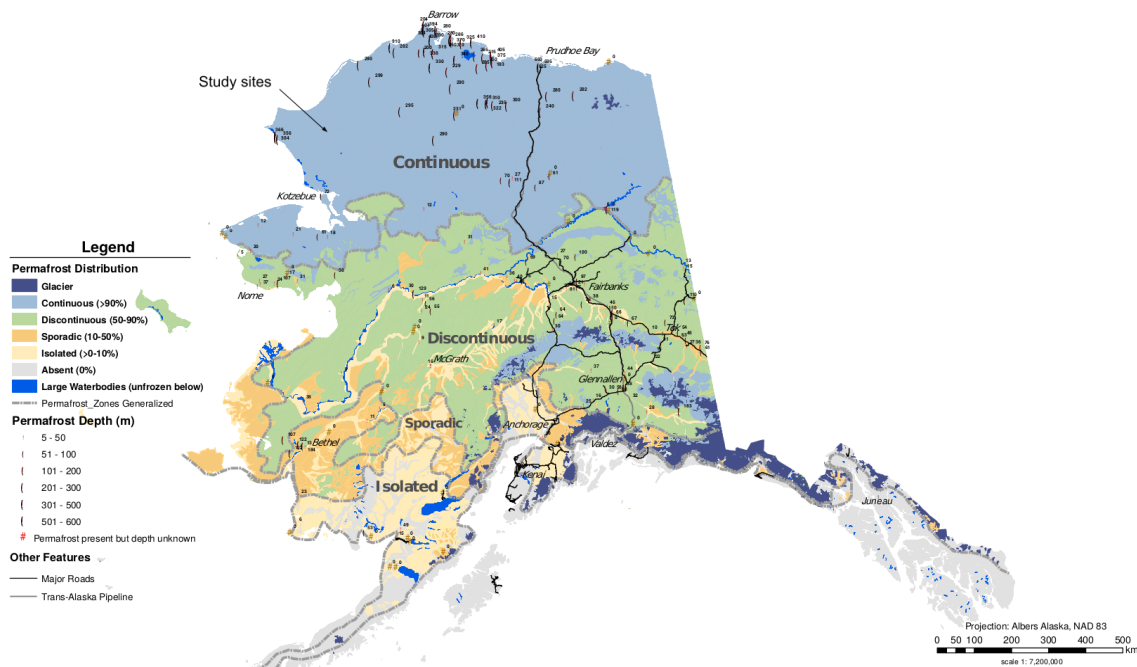


Fig. 1: Distribution of Permafrost in Alaska (Jorgenson et al., 2008)

A large part of the continuous permafrost Arctic landscape and most of the Northern and Western Alaska Lowland is characterized by thermokarst lakes, drained thermokarst lake basins and yedoma (Bergstedt et al., 2021, 1; Jongejans et al., 2018, 6040). At the coastal area of Western Alaska drained thermokarst lake basins dominate. But yedoma, a specific type of permafrost formed in the Pleistocene, is ice-rich and therefore very vulnerable for thawing (Ulrich et al., 2014, 1). Jongejans et al. (2018) did a study on the carbon pools of the different land classes on the Baldwin Peninsula.

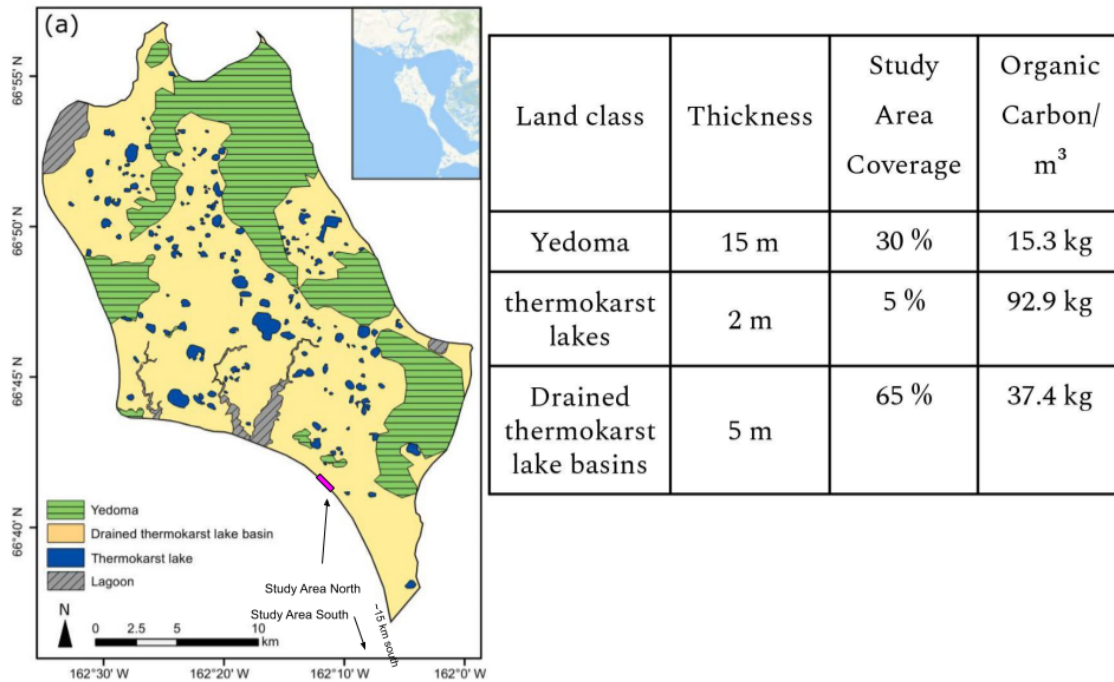


Fig. 2: Land Cover Classification on the Baldwin Peninsula (Jongejans et al., 2018)

Fig. 2 shows the distribution of the different land cover classes and the location of the study sites. Yedoma has less organic carbon per volume, but due to size and thickness of the covered area there is a lot more in total.

In order to calculate the released organic carbon, studies on thawing rates have to be done. But the thawing rate differs a lot by location and type of thawing progress. It can be indicated by different features like thermokarst lake expansion and drainage, forming of polygonal wetland landscapes, active layer detachment slides and coastal erosion triggered retrogressive thaw slumps, which are the research subject of this study.

All the features are either thawing progresses or feedback on them. There are large research gaps concerning their spatial distribution and the timing of the processes. Also wildfires and coastal erosion, the initiative disturbance for retrogressive thaw slumping, are topics of interest because of their influence on permafrost degradation. This big amount of influencing factors and symptoms require a lot of different scientific examinations.

1.1.2 Remote sensing on Arctic permafrost

Remote sensing brings a lot of benefits for researching the Arctic and permafrost regions of the planet. Not only the obvious reasons like minimizing expensive traveling to remote study areas with cold and hardly any infrastructure. But also getting data with a high spatial and temporal resolution makes remote sensing a perfect tool für detecting changes in the polar regions.

Methods differ by use case: For small study areas tools like terrestrial laser scanning or UAVs are used, whereas for big study areas satellites are essential. There are passive sensors measuring the sunlight reflectance of the subjects. Optical remote sensing uses multiple sensors for different wavelengths giving a broad range of information. By using multiple bands for calculation specific indices are developed — for example to measure vegetation changes with the Normalized Difference Vegetation Index (NDVI) (Berger et al., 2020). Active sensors on the other hand emit radiation themselves and measure the reflectance of the observed surface. Radar are well-known tools. Unlike the sunlight the amount of radiation energy can be defined. This makes it possible to measure despite the absence of daylight and the variable cloudiness. It is also used for determining elevation and distance by measuring the time an emitted signal takes to be detected again. Therefore it is widely used for detecting spatial changes like canopy height (Berninger et al., 2019).

Permafrost itself can not be measured by any of these tools, but related variables like vegetation, landscape changes and permafrost features can be detected. In the following some of these will be presented. Land cover and vegetation changes are often researched with both aerial imagery and multispectral satellite data like Landsat, Quickbird and Ikonos. This is done either by calculating indices like the NDVI, the NDMI (Normalized Difference Moisture Index) or by changes in aerial images, which have been available since the 1950s (Jones et al., 2011; Jorgenson et al., 2018). For detecting thermokarst lake changes and drained lake basins, also multispectral remote sensing like Landsat or Planet Cubesat data is used, but also radar data like Sentinel 1 (Bergstedt et al., 2021; Nitze et al., 2020; Paltan et al., 2015). Arctic coastal erosion rates are quantified with airborne lidar and several multispectral data (Jorgenson and Brown, 2005; Obu et al., 2016). Landscape elevation changes due to the subsidence of yedoma permafrost or

erosion of ice-rich riverbanks can be well detected by active satellite tools like TerraSAR-X and differential SAR interferometry. But also stereographic optical imagery is used — for example the Arctic DEM generated by WorldView imagery with a resolution of 5 m (Antonova et al., 2018; Porter et al., 2018; Stettner et al., 2018). To get an even higher resolution airborne LIDAR can be applied. That can bring a vertical resolution of higher than 10 cm (Rettelbach et al., 2021, 4). Another interacting factor on the frozen ground are the more severe and frequently happening wildfires in the high latitudes (Kasischke et al., 2012). Optical remote sensing can be used to determine variables like burn severity or water content of vegetation (Jones et al., 2009, 2013). Another correlation to erosion and thawing processes are changes of the nearshore sea reflectance and turbidity due to washing in of large amounts of sediment (Fig. 3). This can also be detected by multispectral remote sensing (Heim et al., 2014; Klein et al., 2021). Remote sensing on aprub thawing processes and RTS, which are mostly triggered by coastal erosion, are described in detail in the next chapter.



Fig. 3: Sediments washed into the sea close to the study sites at the Baldwin Peninsula at the 3rd of July 2021 (Grosse, 2021)

1.1.3 Retrogressive thaw slumps



Fig. 4: Retrogressive thaw slumps at the Baldwin Peninsula. The central slump has an active slump at the right and an already stabilized part at the left. Underneath the plateau the headwall is seen which is more active at the right. Also the active slump floor is steeper and continues in a sediment flow. Further down at the beach the sediments form a debris cone (Strauss, 2016).

One of the most impressive and dynamic permafrost thaw erosion features are retrogressive thaw slumps (RTS) (Fig. 4). They are initiated by disturbance of ice-rich permafrost ground — mostly erosion by waves or tides at steeply sloping coasts. Once the ice-rich layer is exposed and starts thawing, a steep headwall forms. When the thaw erosion surpasses the coastal erosion, the headwall retrogresses. The eroded sediments and ice wedges form a slowly moving mud flow (Lantuit and Pollard, 2005, 415). Fig. 5 visualizes the typical structure and the above described thawing process.

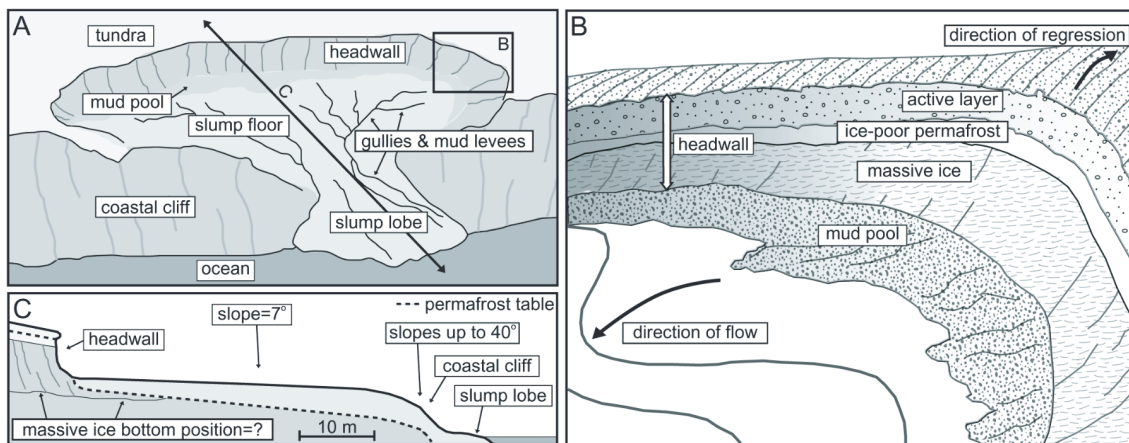


Fig. 5: Structure of a retrogressive thaw slump (Lantuit and Pollard, 2005)

The first remote sensing studies on dynamics of RTS were done based on aerial images and satellite RGBs images. Trends of increasing occurrence and bigger extent were stated, but it was not possible to determine correlations with climate and environmental variables. Brooker et al. (2014) did an analysis with the method of Tasseled Cap Transformation — a specific transformation of spectral Landsat data. They identified RTSs, detected their level of activity, measured rates of headwall retreat and rates of restabilization.

Runge et al. (2022) combined Landsat and Sentinel 2 imagery and calculated annual thaw dynamics of several study sites using the automated change detection algorithm LandTrd. There were strong correlations found between the occurrence of RTSs and environmental factors: RTSs are mostly found at ice-rich permafrost sites at slopes close to the sea- or lakesides (Runge et al., 2022, 11). The abrupt RTSs movements differ a lot from year to year, but there was not any correlation found between annual thawing rates and climate variables like annual precipitation, summer precipitation or thawing days (Runge et al., 2022, 13). In contrast to that Lewkowicz and Way (2019) determined a strong connection between thawing rates and temperatures in the summer months.

The carbon release is currently only modeled for the gradual thawing of permafrost regions at a global scale, but abrupt thawing processes like RTSs are not included. Turetsky et al. (2020) estimate that their impact will be quite big in the near future.

Therefore it needs to be better understood which climate drivers trigger abrupt RTSs and how much carbon is released by them in total.

1.1.4 Climate change related increasing of precipitation

Poujol et al., (2020) developed a thermodynamic model for the future climate in Alaska. It states that convective storms will not be restricted to the area south of the Yukon River anymore. They will also appear at the North Slope and Westcoast. Precipitation will get more intense and may cause flash floods. Also mean precipitation increased for the last decades and may also continue with climate change as well. As shown in Fig. 6 especially the South- and Westcoast received an increase of precipitation since 1970 of about 20 %. Especially in Kotzebue at the Baldwin Peninsula the mean annual precipitation increased over the last decades - the mean trend changed from 250 mm in 1977 to about 300 mm in 2010 per year (Fig. 7) (Necsoiu et al., 2013). But it is not that easy if it will continue that way or not because precipitation trends depend on a lot of different factors. For the region of Alaska also declining sea ice extent and the availability of open coastal water is relatively important. Probably the most important factor for precipitation is the sea water temperature and changes caused by the Pacific Decadal Oscillation, a phenomenon which works similar to the better known El Niño Southern Oscillation (Wendler et al., 2017, 3ff).

High precipitation and especially heavy rain events amplify coastal erosion (Marzen et al., 2017; Young et al., 2021). This triggers rapid retrogressive thaw slumping (Lantuit and Pollard, 2005).

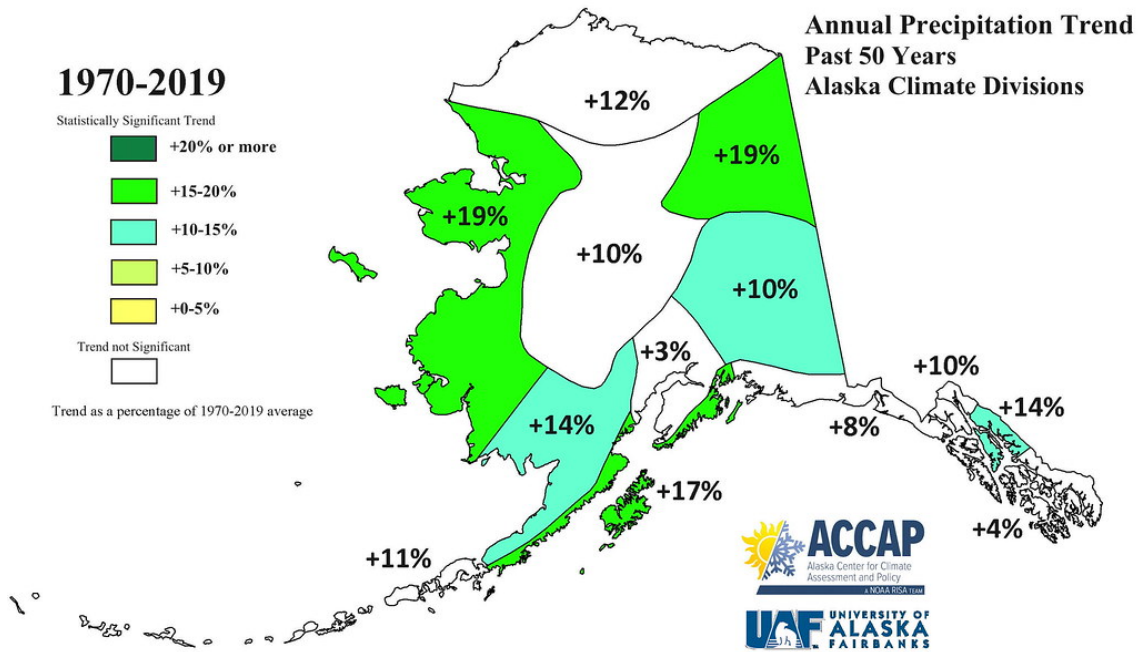


Fig. 6: Precipitation Trend in Alaska (Alaska Center for Climate Assessment & Policy, University of Alaska Fairbanks, funded by the NOAA Climate Program Office, 2022)

Kotzebue mean annual precipitation

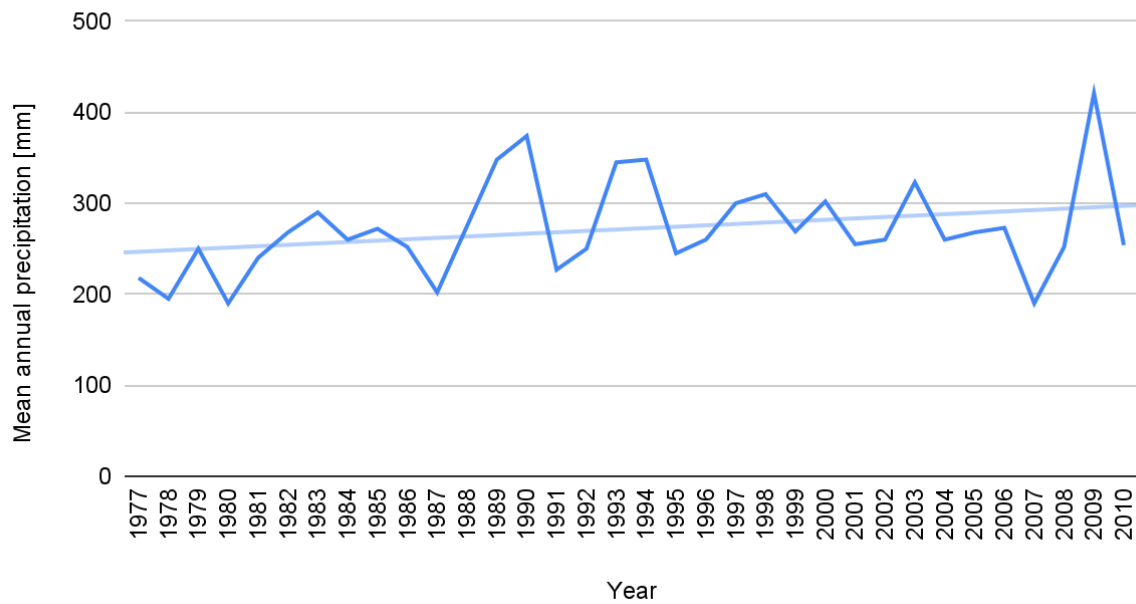


Fig. 7: Last decades' mean annual precipitation in Kotzebue on the Baldwin Peninsula (Necsoiu et al., 2013)

1.2 Usability of MACS imagery for DEM differencing

To get more precise information about the dynamics of RTSs it is indispensable to get data with a high spatial resolution (centimeter range). But data with that accuracy is mostly only available for small study sites — for example measured with UAV photogrammetry by Van der Sluijs et al. (2018). To get usable information the data should be available for a whole coast section — means several hundred meters or kilometers — because at small sites the environmental factors differ too much with respect to active layer thickness, ice content, hydrology and slope.

The already available data for large areas does not have a high enough spatial and temporal resolution: E.g. There is the circum-Arctic ArticDEM with a 2 meter spatial resolution created every two years and therefore not sufficient. Paine et al. (2013) used airborne Lidar for creating a DEM with 0.25 m resolution. They mapped thermokarst lakes and pingos at Alaska's North Slope Plain. With this data elevation changes and movements can be detected in an adequate way. This could probably also be applied for RTSs.

In order to find out influences of rainfall and especially heavy rainfall events as described in the previous chapter, it is important to have a better temporal resolution. For the summer months a regular data acquisition is necessary to detect the influences of such events. Fortunately there were record breaking strong rainfalls at the time of the Perma-X 2021 Flight Campaign (June and July 2021) in Western Alaska. For Kotzebue (Western Alaska) July 2021 was the wettest month ever recorded: The precipitation was 135.1 mm (Alaska Center for Climate Assessment & Policy, University of Alaska Fairbanks, funded by the NOAA Climate Program Office, 2022a). Also in Kotzebue, on the 6th and 7th of July 2021 the highest 24-hour precipitation ever was registered (Alaska Center for Climate Assessment & Policy, University of Alaska Fairbanks, funded by the NOAA Climate Program Office, 2022b). For the aim of the study - to detect differences - this coincidence of strong rainfall and therefore erosion was a big benefit.

Our attempt in this study is to use MACs airborne stereo imagery for creating DTMs on two study sites by Structure-from-Motion photogrammetry with a high spatial

resolution. Then DTM differences of two respectively three different days are calculated to quantify mass movement and thaw slumping.

To apply this method on the data several preparation steps and a specific processing workflow was developed which will be described in the following chapter of methods and data. Afterwards results and errors are presented and it is going to be discussed whether the data and the develop workflow are sufficient enough to measure changes accurately or not.

1.3 Study Sites

The two study sites are both located at the coast of the Baldwin Peninsula south of the Kotzebue in Western Alaska (Fig. 8) they are about 66° North and underlain by continuous permafrost. Study Area South (SA South) is just 4 km north of the Arctic Circle and Study Area North (SA North) about 12 km north of SA South. SA South's dimensions are 1300 x 220 m - SA North's 960 x 160 m.

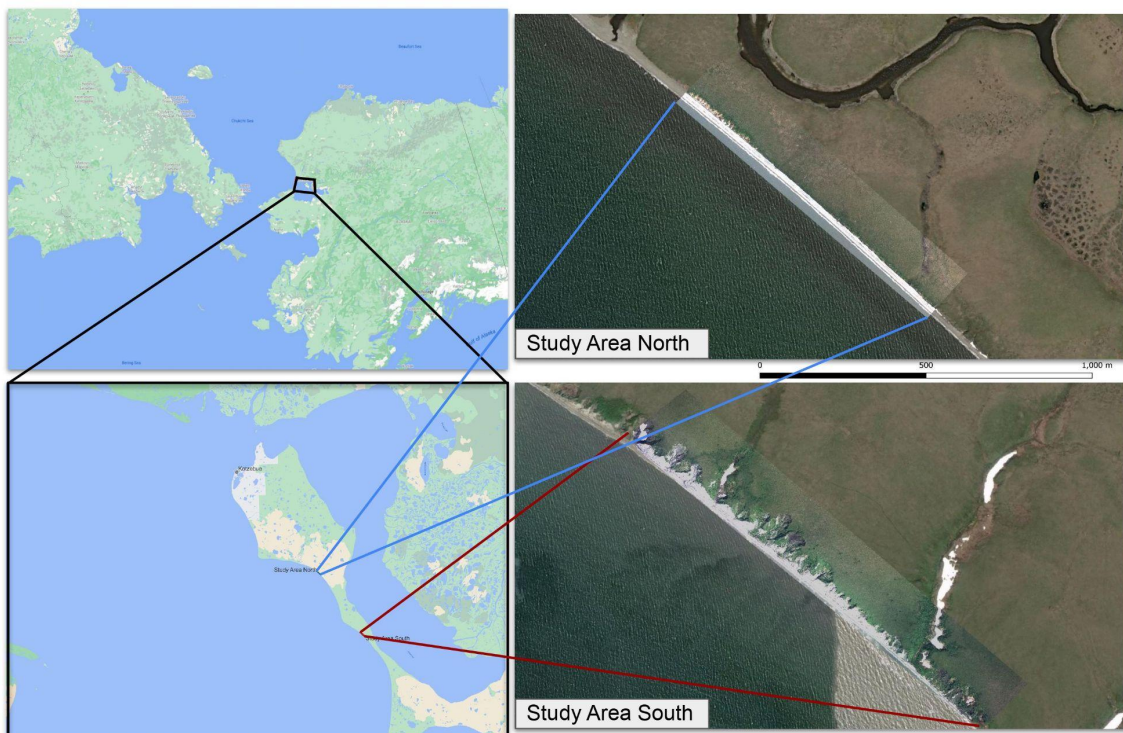


Fig. 8: Location of study sites. Background maps are provided by Google (Google Maps, 2022)

The study sites were chosen in similar size covering a few hundred meters of Arctic permafrost coast. The exact position of them derives from the covered area of the 2021 Perma-X flight campaign (Fig. 9). The different temporal resolution and orientation of the flights led to the two selected study areas. SA South was observed on the 3rd and 10th of July 2021 — SA North on the 28th of June, 3rd and 10th of July 2021.

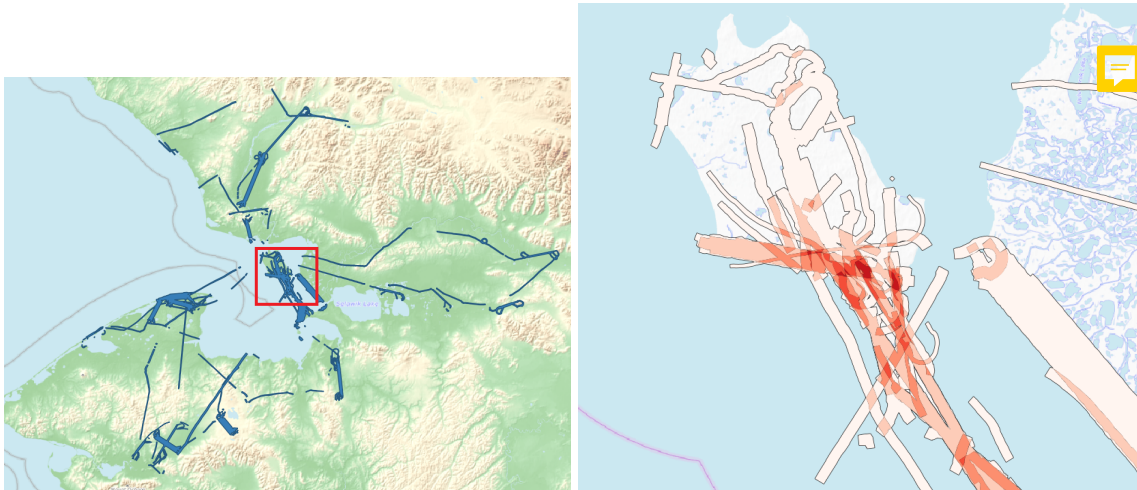


Fig. 9: MACS footprints of PermaX 2021 flight campaign (Nitze, 2021)

The ortho mosaics of Fig. _ shows that SA South has a steep coast while SA North is pretty flat. At SA South the plateau is about 40 m above sea level whereas at SA North it is just eight meters difference. SA South's permafrost degradation features and thaw slumps can be recognized well. There is most likely ice-rich yedoma permafrost underneath (see 1.1.1). SA North's ortho mosaic, which is at the exact same scale, shows much less degradation processes. There is also some coastal erosion and gullies, but large retrogressive thaw slumps and slides can not be seen. Jongejans et al. (2018) classified this area as drained thermokarst lake basins (see 1.1.1).

2. Methods and material

2.1 Workflow

The created workflow to fulfill the study's objectives is presented in this chapter of methods and material. It is about the MACS data, the pre-processing, the processing of the imagery to create digital terrain models and ortho mosaics, the applied

co-registration and the calculation of DTM differences. In Fig. 10 all steps of the workflow are presented in an overview giving flowchart.

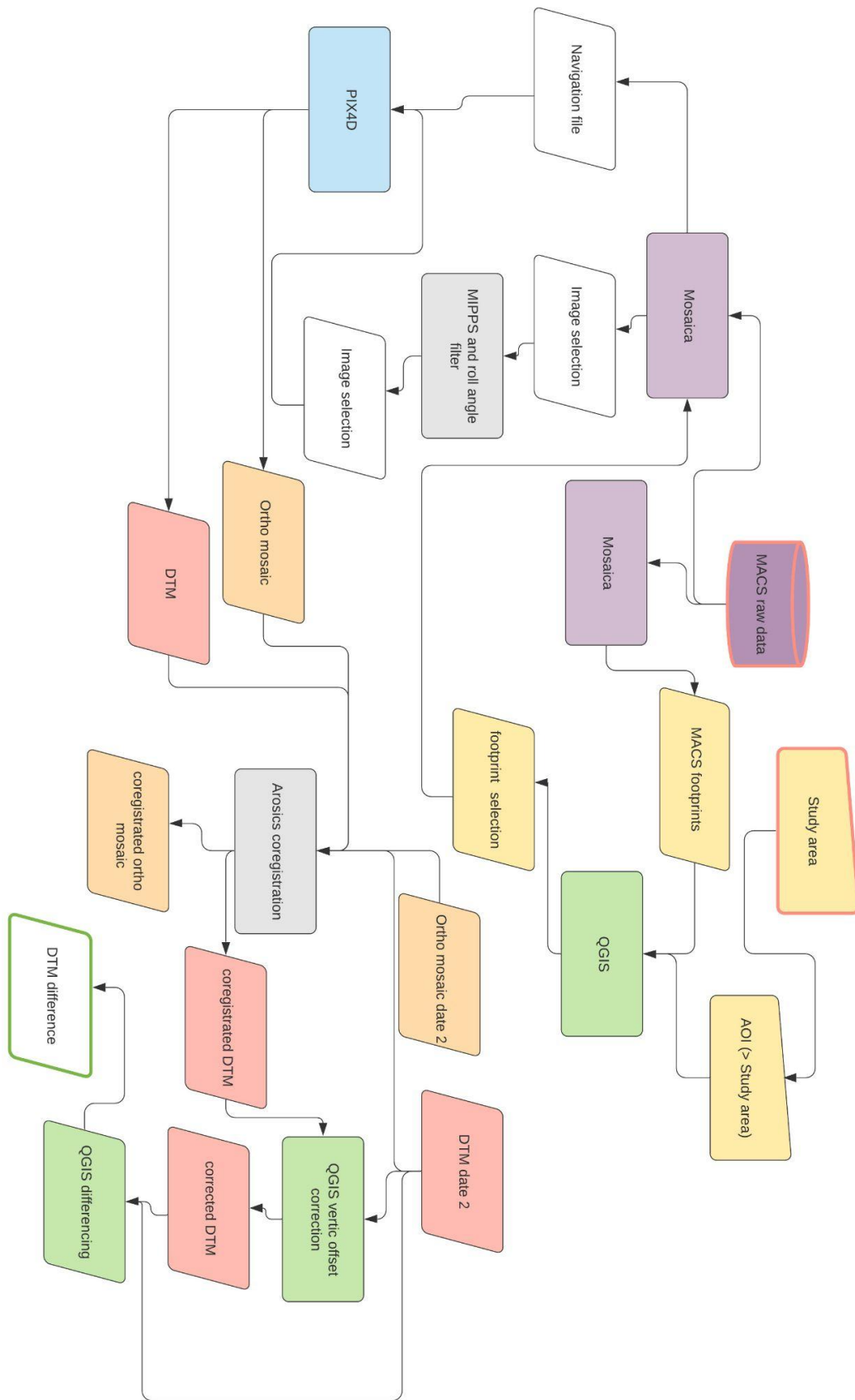


Fig. 10: Flowchart of the developed workflow

2.2 MACS airborne data

The image data was collected within the scope of the Perma-X flight campaign in June and July 2021. The flights were done with the AWI Polar-6, a Basler BT-67. The MACS (Modular Aerial Camera System) Polar 18 is a camera system for researching the polar regions, developed by the DLR (German Aerospace Center) Institute of Optical Sensor Systems. It records imagery in both visible wavelength range (RGB) and near-infrared range (NIR) at a flying altitude between 1000 and 1500 m. Areas of interest were different permafrost landscapes and features like coastal erosion, ice-wedge degradation, fire scars, thermokarst lake changes and pingos but also settlements and infrastructure. Most of the flights were done over and around the Baldwin Peninsula (Fig. 9).

At both study sites data was collected in a pattern with an overlap of more than 80 % and also from different flight directions. In early trials it was found that this reduces the risk of distortion. For the study only RGB-imagery and no NIR was used, because the resolution is higher and also true color ortho mosaics are also needed. The left image of Fig. 11 A shows the images taken during a flight on the 3rd of July 2021. For better processing results the image selections were chosen quite a bit bigger than the study areas (Fig. 11 B a. C). The automatic matching of images within the study areas works significantly better when all overlapping pictures are taken into account as well. All the images have a size of 4864 x 3232 pixels.

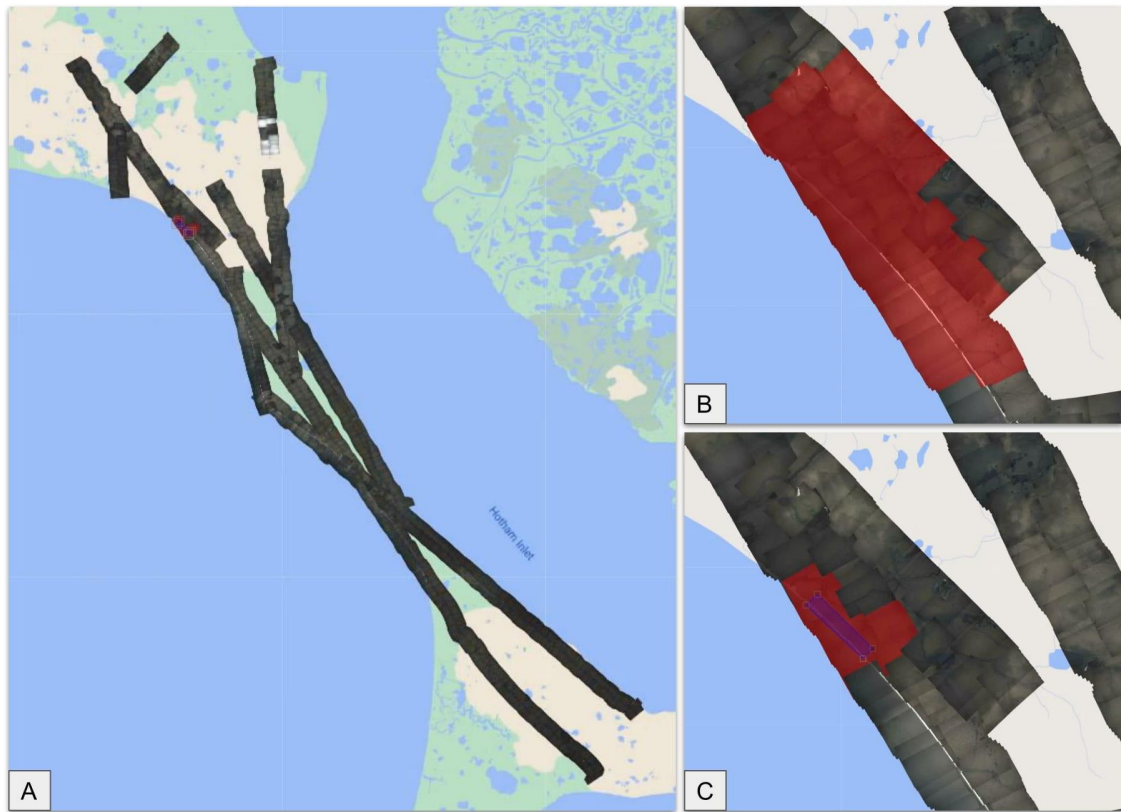


Fig. 11: Image selection for SA North; A) All images of the flight on 3rd of July 2021; B) 104 images covering SA North; C) SA North actual size. Background maps are provided by Google (Google Maps, 2022)

2.3 Data pre-processing

For each MACs image a shapefile of its footprint exists in the database. Via GIS the specific footprints can be selected by a shapefile. A Python script by Nitze and Rettelbach (2021) creates a processing directory and copies the TIFF files, which are covered by the previously selected footprint files, from the database to the directory. For SA South 109 to 114 images were selected - for SA North 78 to 104. Then the images were filtered by a maximum roll angle. If the roll angle of the aircraft is too large at the time the image was taken ($> 3^\circ$), it is probably distorted and should not be taken into account (Ruzgiene, 2014, 101). The script also corrects the attribute order of the navigation file which is important for photogrammetric processing. For generating the ortho mosaic from the MACS imagery the DLR created several image filtering and stretching tools combined in the 'MIPPS' toolbox. For these images the Debayer filter optimizes the color range and the Devignetting repairs the brightness reduction at the edge of the images. It is also integrated in the pre-processing python script.

2.4 Progressing and point cloud classification

The photogrammetric processing was done with the software PIX4Dmapper. PIX4D is a photogrammetry software. It combines multiple overlapping images to an orthomosaic by detecting keypoints. A keypoint is a point, which can be identified as the same in several images. For the 3D-surface-model a 3D-point-cloud is created in the first place. PIX4D knows the camera position, angle and distance between a keypoint and the camera. If a keypoint is detected in several images, the software can calculate the points position in 3D-space by triangulation. Fig. 12 describes the method.

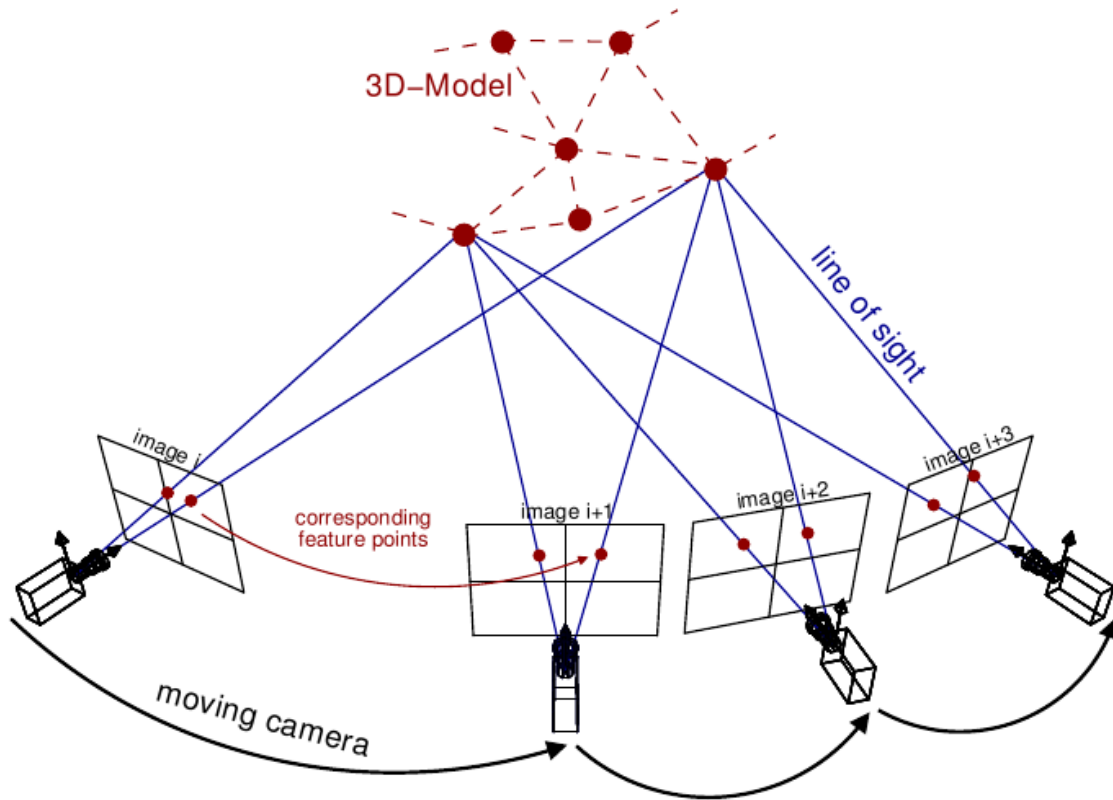


Fig. 12: Structure-from-motion principle (Sweeney, 2016)

By finding several thousands of keypoint per pair of images, an error detection and correcting of the camera's position and orientation can be done as well, which can even improve the result (Hawkins, 2016, 10).

For setting up the PIX4D Project the previously created directory was helpful for keeping the overview. At first the input images were selected and the update navigation information added. All images were now assigned as geolocated. Also it was checked if the right camera model was selected. At the end of setting up, '3D Model' instead of "3D map" was selected, because the results of the DTM are more accurate..

The processing progress is divided in three parts: '1. Initial Processing', '2. Point Cloud and Mesh' and '3. DSM, Orthomosaic and Index'. They all have their own settings and can be run individually after the previous steps are done. Step 1 and 2 can be run at once. The 'General', 'Matching' and 'Calibration' settings of step 1 can be kept on default, whereas in step 2 'Point Cloud Classification' image scale should be switched to '1' and Point Density to 'High'. Also 'Classify Point Cloud' should be checked to improve

results. After executing the first two processing steps a look at rayCloud and the generated 3D-point-cloud should be done: Major distortion problems can be seen here if they occur. Also problems with the camera settings / view angles or matching of images by finding enough key points can be detected.

In the settings for step 3 'Additional Outputs' Raster DTM must be checked. A DTM (Digital Terrain Model) is a filtered DSM (digital surface model), where only points declared as 'Ground' and 'Road Surface' in the classified Point Cloud are taken into account. The DTM is much more applicable for our purpose than the DSM because a lot of error points are also generated in the DSM, but mostly automatically classified as 'Building' or 'High Vegetation' (Fig. 13). Most dislocated points are at well vegetated ridges and hilltops (declared as 'High Vegetation') and at the steep vegetation-free slopes (declared as 'Building'). The output DSM of an unfiltered point cloud can be seen in Fig. 14. The errors at the slope are severe. Only the flatter debris flow part of the steep coast looks fine.

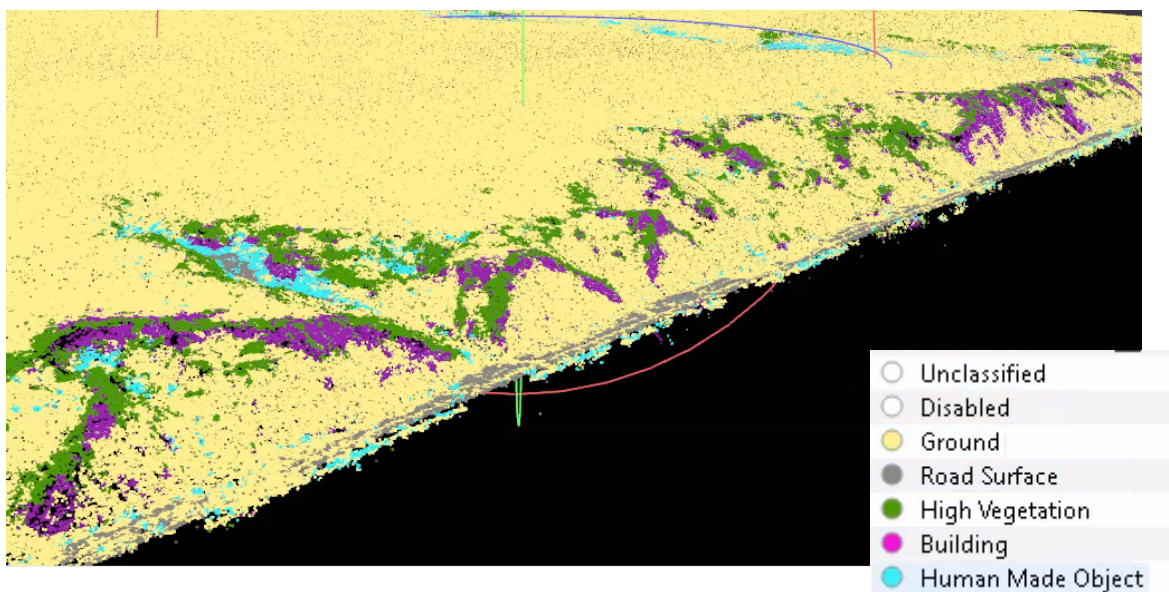


Fig. 13: Automatically classified point cloud in PIX4D

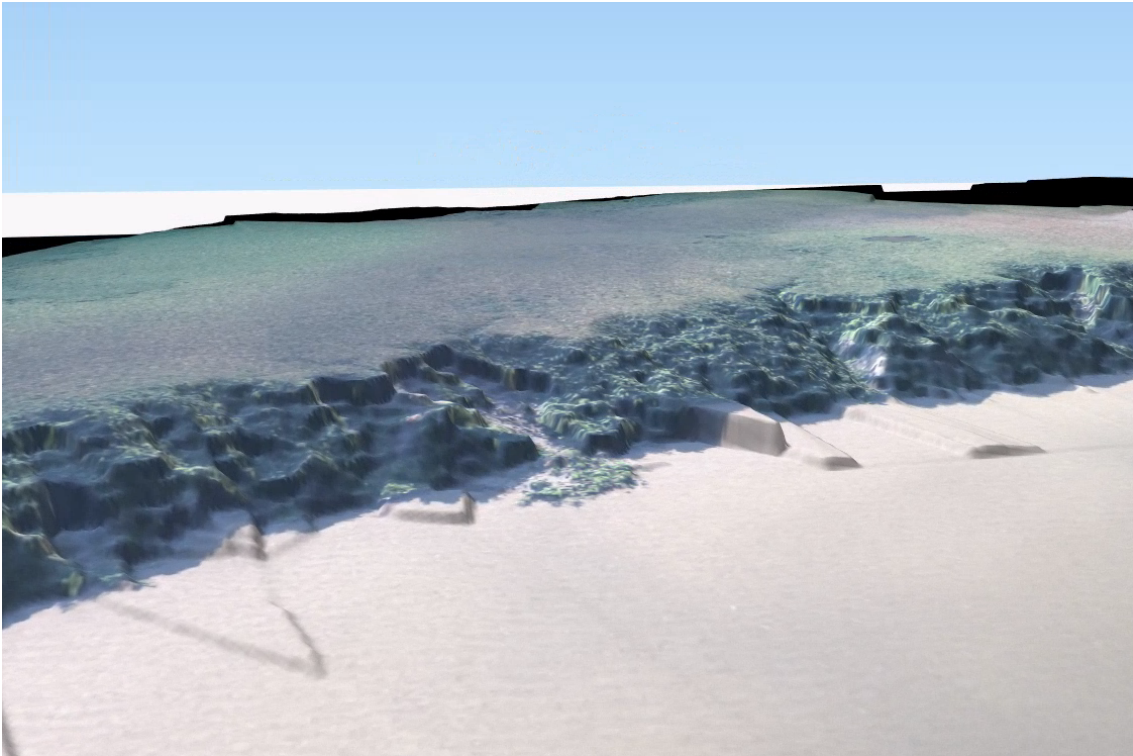


Fig. 14: Defective 3D-DSM

2.4 Image co-Registration

In order to calculate elevation differences of the DTM, the images have to be exactly spatially aligned. But due to different factors they have got a natural offset which differs within the images. To reduce this deviation to a minimum, the images have to be coregistered. There are different methods working by using the ortho mosaic for detecting the spatial difference and applying the transformation to the DTM.

The most common one is the QGIS 'Georeferencer' tool. Basically the method works by choosing Ground Control Points (GCPs) which are set at distinctive pixels. This GCP must be aligned to its equivalent in the other picture. There are several different transformation types used for different kinds and levels of distortions. The modern 'Thin Plate Spline' transformation works best for our data because it can sort out both different local deformations and general offsets.

For the MACS imagery an even more accurate tool than 'Georeferencer' is the DLR-tool 'AROSICS', an 'Automated and Robust Open-Source Image Co-Registration Software for Multi-Sensor Satellite Data' developed by Scheffler et al. (2017). The local

co-registration algorithm applies a moving-window detecting local displacements and calculates a grid of local shifts using tie points. There is also the global co-registration algorithm, but it only calculates the offset at a single point and shifts the whole image by this displacement vector. The global approach is computationally less intensive, but this is not relevant at this stage (Scheffler et al., 2017, 5).

To decide which method should be applied in this study, all of them were tested at both study sites. The 'Georeferencer' 'Thin Plate Spline' did not work out that well and the result was still pretty displaced some parts of it. Also the manual selection of GCPs takes a lot of time and is not that accurate in a landscape without solid objects like buildings or rocks. The variable states of light exposure and different vegetation growth make it hard to find accurate points too.

The global and local Arosics approach was tested and the offsets between the output image and the reference image were calculated. The mean offset of the Local AROSICS Algorithm was by far the least. Fig. 15 presents the original displacement for several points and the offset after the global and local co-registration. The points are sorted by their geographic latitude and it can be seen that the original offset becomes larger to the north.

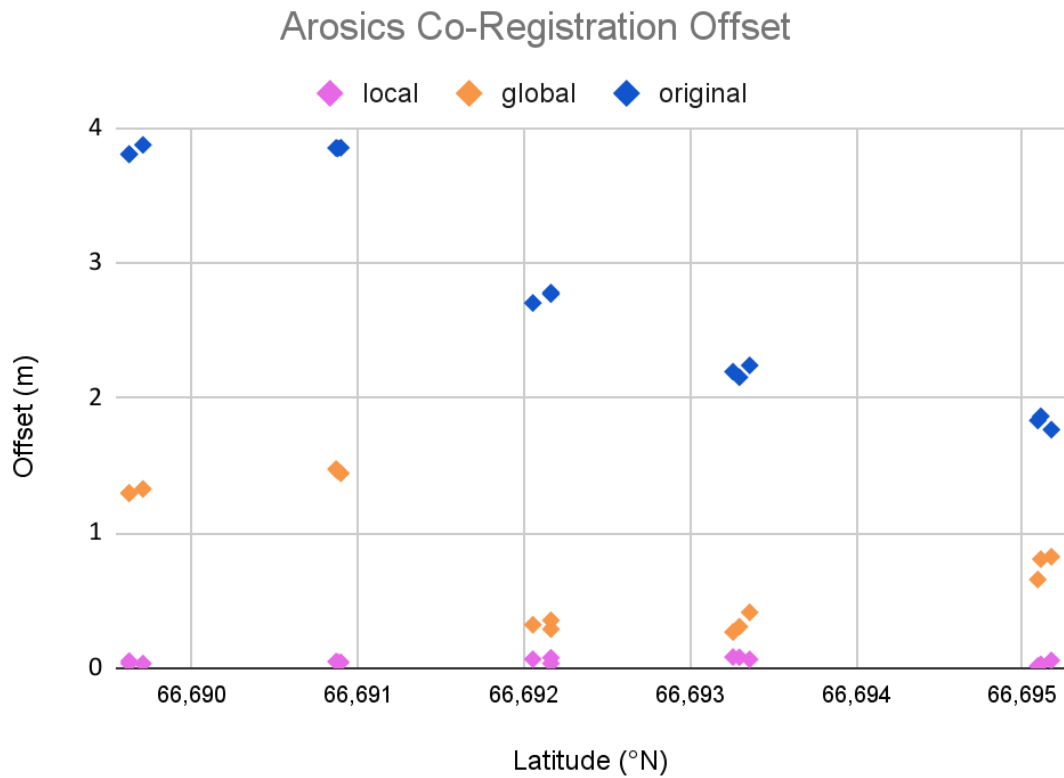


Fig. 15: Comparison of Arosics co-registration offset – global and local

2.5 DTM differencing

After applying the transformation also to the DTM, the quality was checked again by creating profiles in different directions across specific terrain features like small trenches and hills. To visualize the DTM, the QGIS Plugin 'Qgis2threejs' is used. There are also vertical offsets between the dates due to processing failures which have to be corrected (Fig. 16).

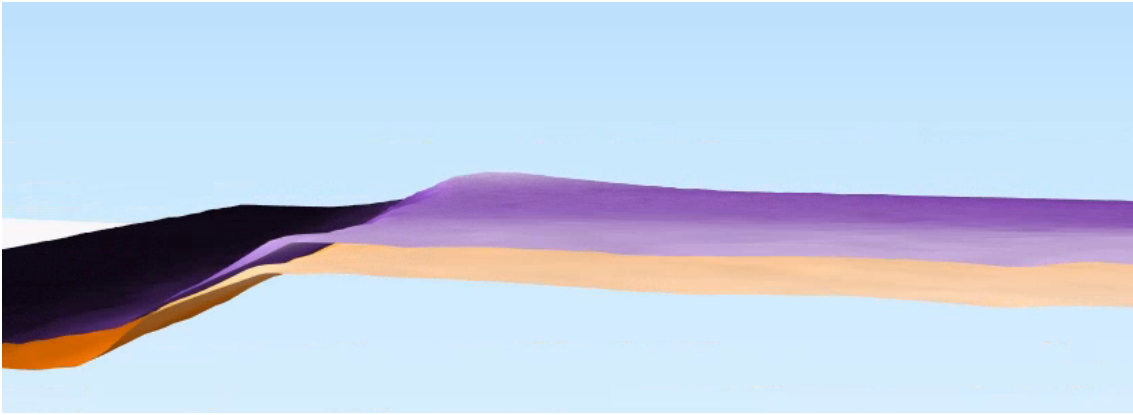


Fig. 16: Vertical offset between 28th of June 2021 and 3rd of July at SA North 2021

To determine it, the mean elevation of the not changing plateau was calculated. In our study the flat area above the coastal slope, where nearly no erosion rates and fast thawing is expected, was taken into account. The difference of the mean elevations, calculated with the QGIS raster layer statistics algorithm, can now be used for adjusting the elevation with the QGIS raster calculator. After that this tool is also used for calculating the DTM differences, which are presented hereafter.

3. Results

3.1 Overview

Our research question was, how usable the airborne MACS Imagery is for measuring mass movement indicating elevation changes, specifically retrogressive thaw slumps. To give a satisfying answer to this objective firstly the results of the DTM differencing of both study sites are being described. Afterwards the changes are interpreted by the knowledge about RTS movement, observations in the ortho mosaic and appearing errors.

3.2 Changes at SA South

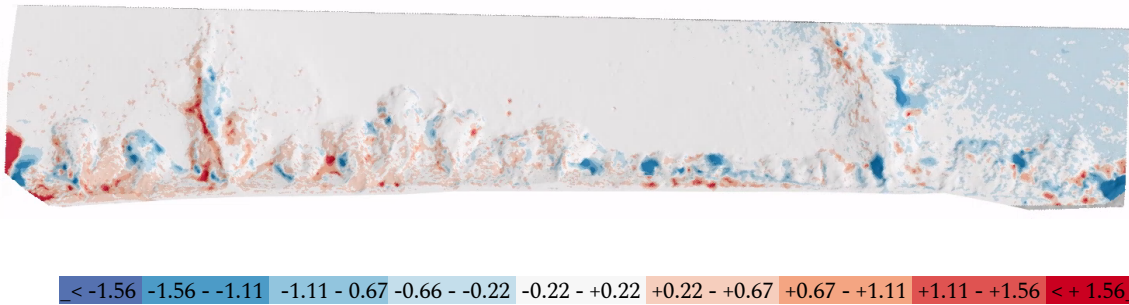


Fig. 17: DTM differencing at SA South on the hillshade of the 10th of July 2021

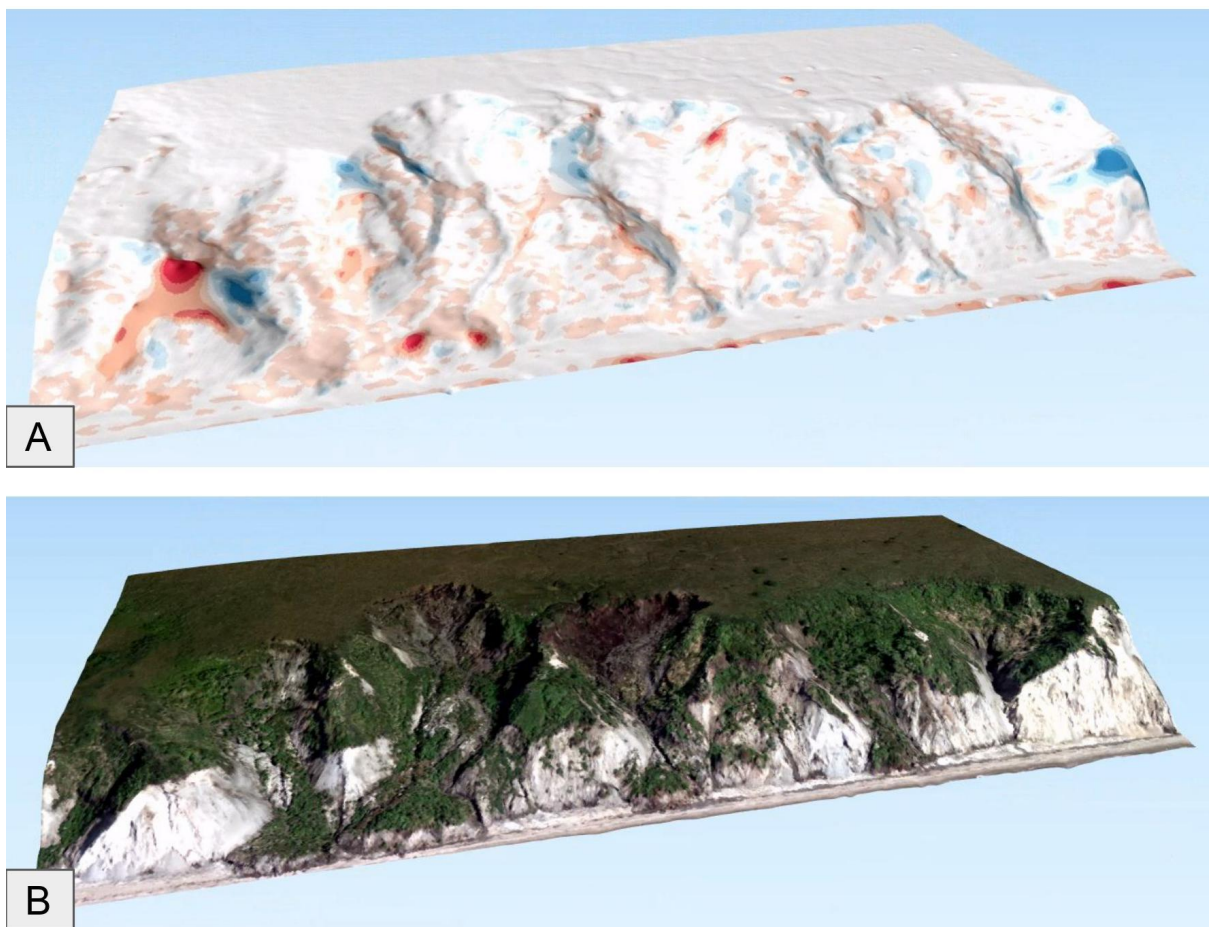


Fig. 18: 3D-Detail of DTM SA South of July 10th 2021; A: DTM covered with DTM difference layer; B: DTM covered with ortho mosaic

The difference image of SA South (Fig. 17), which was created by subtracting the July 10th 2021 image of the July 3rd 2021 image, shows the measured elevation changes. The attached color ramp for indicating the elevation change is also used for several other

figures in this thesis. Great negative changes (> 0.66 m) are mostly detected at ridges between RTS, at the slumps' headwalls and slightly at some other steeper sections of the slope. This can be seen even better at the detailed change illustration laid over the 3D-DTM of July 10th 2021 (Fig. 18). Further down the debris flow the elevation increased. This can be explained by the expected dynamics of the RTS (see. 1.1.3). But there are also a lot of small (< 0.66 m) increasing and decreasing sections apparently randomly distributed all over the slope.

3.3 Errors at SA South

There are also big changes (> 1.56 m) which can not be explained by any natural movement — especially the rising elevation at places where nothing can accumulate because of their exposure like at the left side of Fig. 18. At the whole study site, there are also other locations with eye-catching changes like at the seaside end of the small valley to the left (north) side (Fig. 17). It seems like the red area is the eroded mass of the blue-colored ridge above (Fig 19). But a look at the ortho mosaic DTM combination from the 10th of July 2021 shows that the area is well covered with vegetation and does not show any signs of active mass movement (Fig 19).

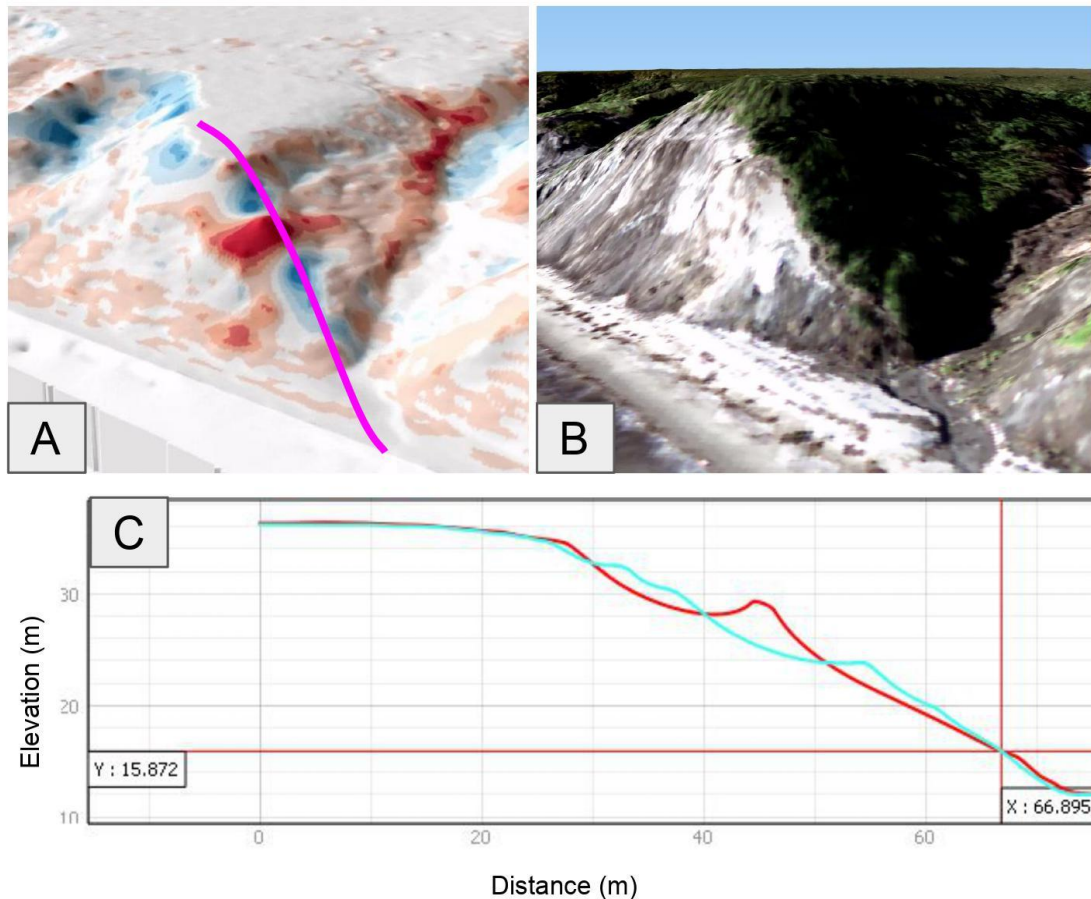


Fig. 19: DTM failure; A) DTM Profile Line; B) DTM covered with the ortho mosaic of the 10th of July 2021; C) Profile of the DTM of the 3rd of July 2021 (Blue) and the 10th of July 2021 (Red)

This leads to the conclusion that at least one of the DTMs has an error at this location. But this failure is not an individual case. They are also occurring at the right (southern) part. Fig. 20 shows the DTM of the 10th of July 2021 covered with the ortho mosaic and the DTM difference. At the left (northern) side some realistic DTM differences with a usual top down movement can be seen. The red areas at the ridge in the middle of the picture and the dominant dark blue area indicate unrealistic high changes at these locations. Further back on the right site some melting snow is seen. There the elevation also decreased.

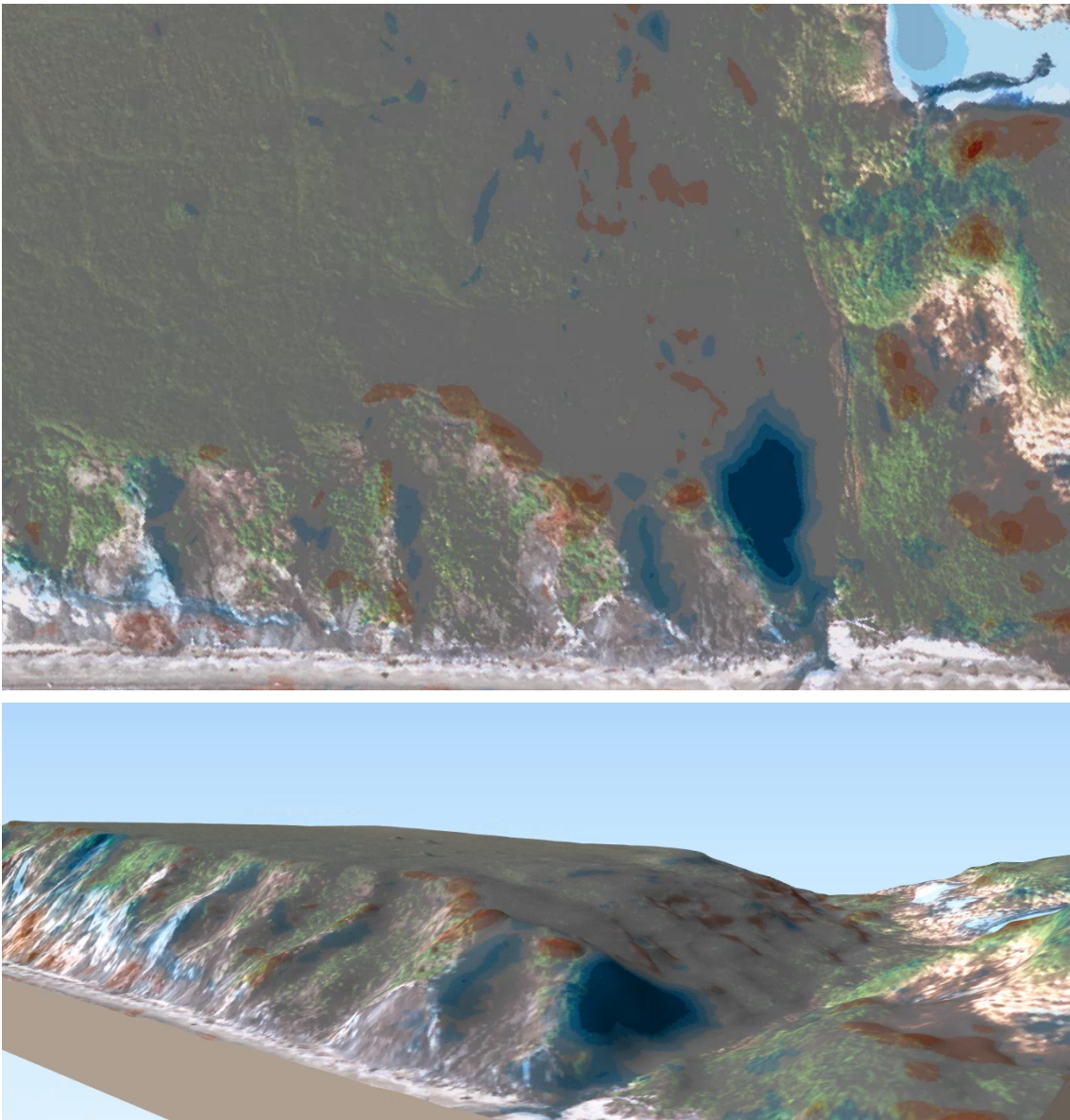


Fig. 20: DTM of the 10th of July 2021 covered with the ortho mosaic and DTM difference

Another occurring error is at the southern (right) flat area above the coast. It is slightly decreasing all over - indicated in blue (Fig. 17). An analysis with the QGIS Profile Tool also shows that most of the flat area lies at the same elevation, but the southern area has an average vertical offset of 0.2 m (Fig. 21).

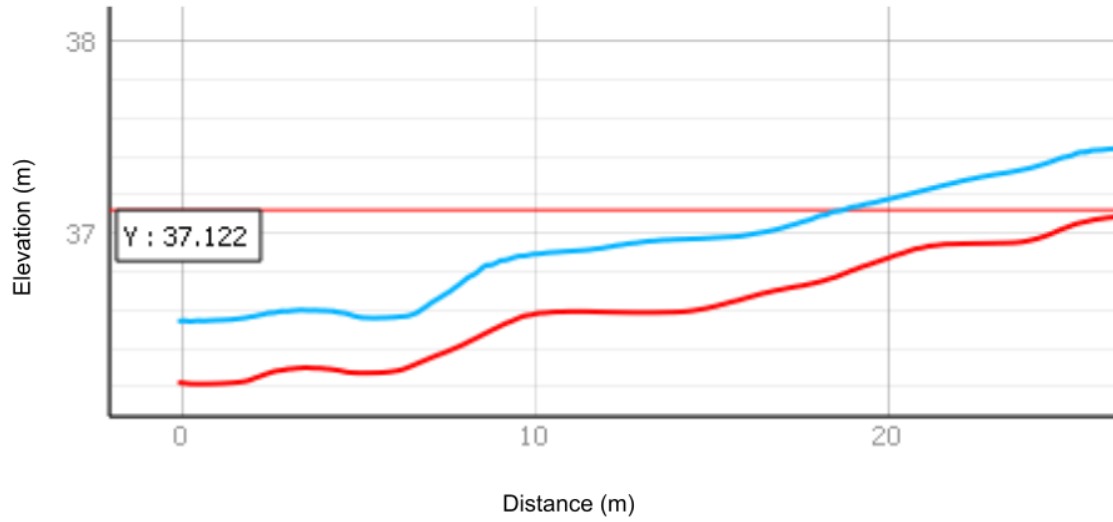


Fig. 21: Vertical offset seen in the profile of the southern area of SA North. Blue: 3rd of July 2021, Red: 10th of July 2021

3.4 Changes at SA North

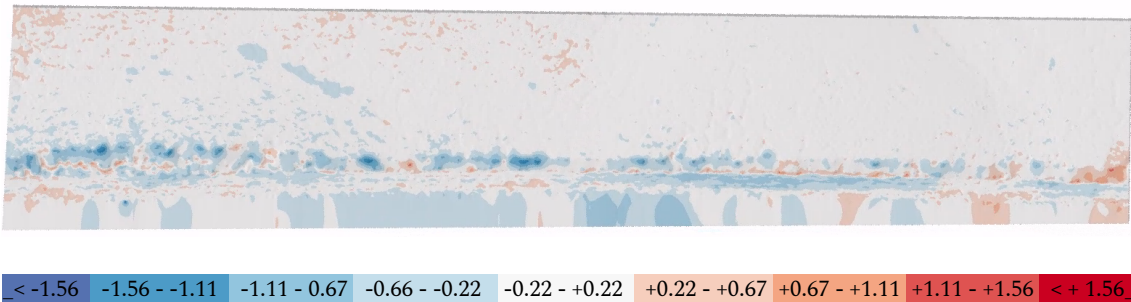


Fig. 22: DTM differencing SA North between the 28th of June 2021 and the 3rd of July 2021 on the hillshade of the 3rd of July 2021

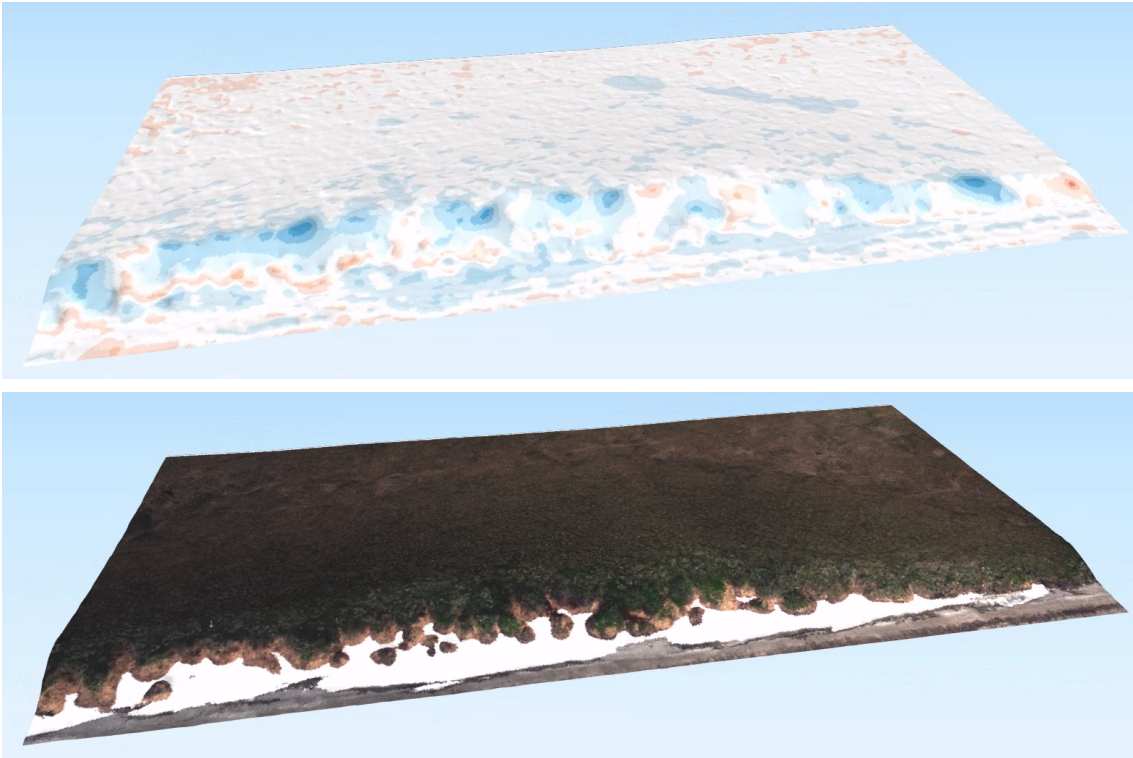


Fig. 23: 3D-Detail of DTM SA South of July 3rd 2021; A: DTM covered with DTM difference layer; B: DTM covered with ortho mosaic

Fig. 22 shows the difference between 28th June 2021 and July 3rd 2021 at SA North. Most of the changes at the coastal slope, which is a lot flatter than at SA South (see 1.3 Study sites), are negative. At the lower area underneath the slope elevation increases at some points.

By taking a closer look in Fig. 23, it can be seen that the biggest decrease occurs at the eroding edge of the cliff and, due to the deposits, the increase is just beneath this area. This is a typical cliff erosion dynamic (Obu et al., 2017, 10). The ortho mosaics of the 28th of June 2021 shows that the decreasing elevation between the debris and the sea is found to be snow, which was melting at this time (Fig. 23).

3.5 Errors at SA North

For the SA North, there was also data collected on a third date. The image below shows the difference between 3rd and 10th of July 2021. Contrary to our expectations most of the slope decreased except for an area on the left (north) side (Fig. 24).

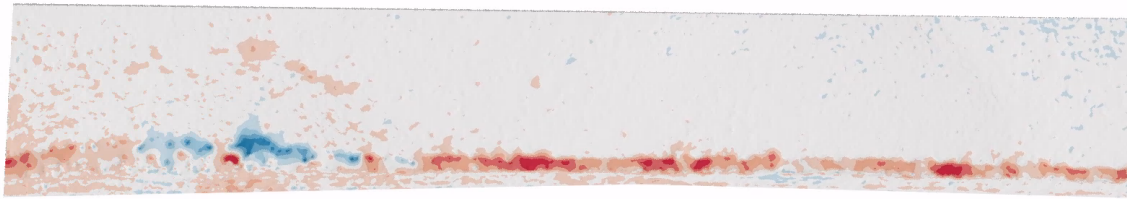


Fig. 24: DTM differencing SA North between the 3rd and the 10th of July

The cross section shows that the DTM of July 10th 2021 (red) is situated about one meter higher than the one of the 3rd of July 2021 (Fig. 25). This is about the same in the entire right two thirds of the image.

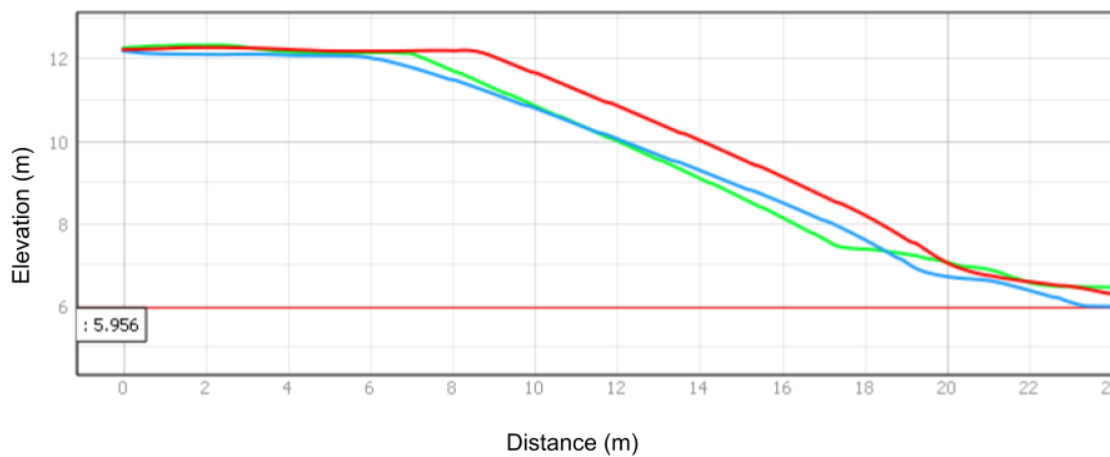


Fig. 25: Profile of the right $\frac{2}{3}$ of the DTMs at SA North of the 28th of June 2021 (Green), 3rd of July 2021 (Blue) and 10th of July 2021 (Red)

At the left side, the result of decreasing, corresponds to the expectations, but it is also more than one meter vertical offset (Fig. 26). This is higher than a realistic change during this short period (Obu et al., 2017, 10).

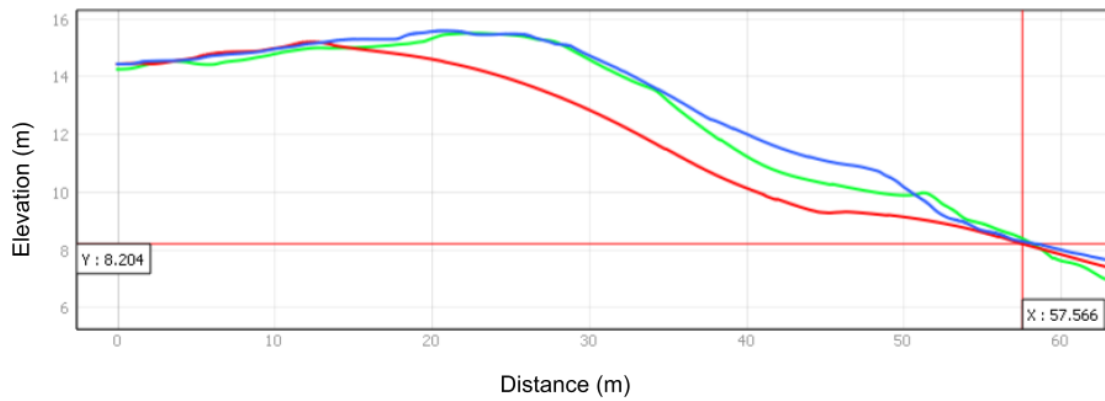


Fig. 26: Profile of the left third of the DTMs at SA North of the 28th of June 2021 (Green), 3rd of July 2021 (Blue) and 10th of July 2021 (Red)

3.6 Processing errors

In addition to the previously described failures several others already occurred during the processing of the data. For example, an additional study site just south of Study Areas North was also initially considered. But the DTM for the 10th of July 2021 had a strong tilt (Fig. 27). Due to that a successful DTM differencing could not be done at this study area (Fig. 28).

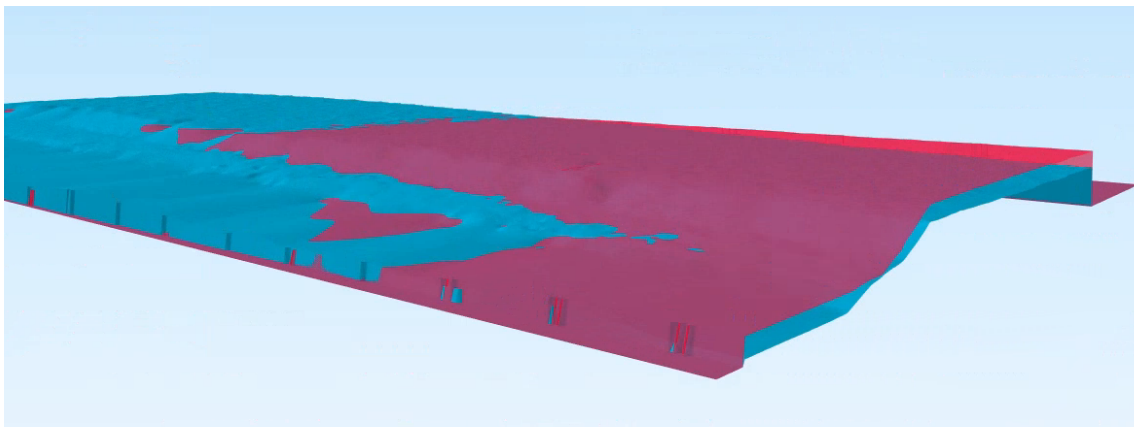
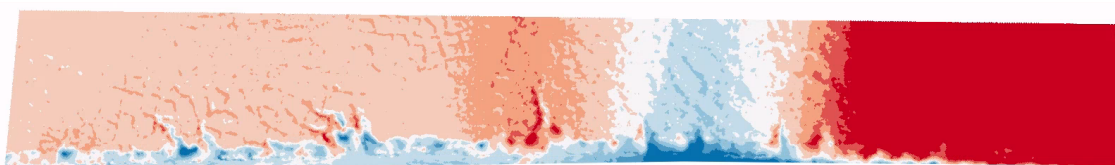


Fig. 27: Even DTM of the 3rd of July 2021 (Blue) and tilted DTM of the 10th of July 2021



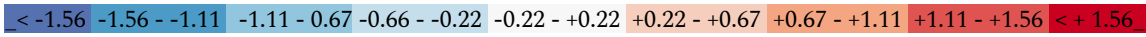


Fig. 28: DTM difference at an extra SA between 3rd and 10th of July 2021

Another possible study site dropped out because the matching of the images in PIX4D did not work out well as the images were partly far displaced. In the point cloud, it can be seen that this area was tilted, aswell (Fig. 29).

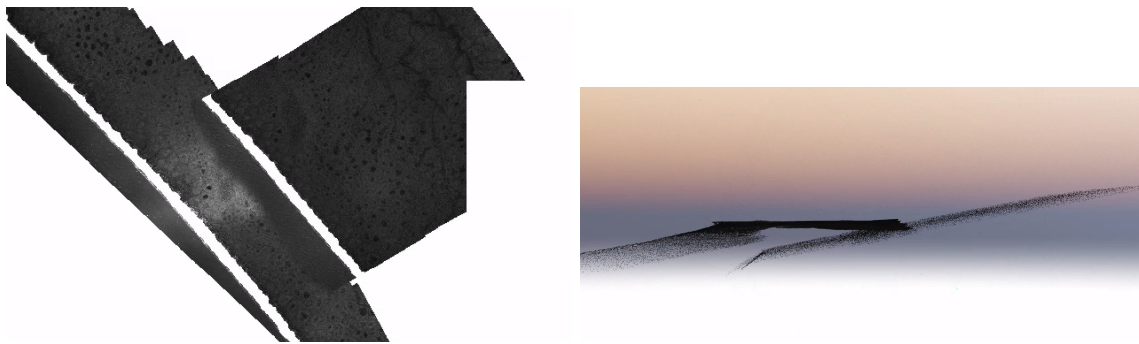


Fig. 29: Displaced image parts caused by matching failures

According to several trials, this happens when the image availability is not good enough, because either the flight data was not collected lattice-like, too many images were sorted out due to a high roll angle or to a too small overlap. Luckily the matching errors can already be seen after the first processing step of PIX4D.

4. Discussion

In the end, it must be said that the combination of the data and the created workflow are not sufficient for the objective to measure elevation differences. The data was collected at the good time — before and after heavy rainfalls, which are believed to trigger erosion and retrogressive thaw slumping. Movement can be seen in the ortho mosaics and at certain points of the DTM. But in all DTMs too many and severe errors occur. This makes it impossible to detect thaw slumping rates, not to mention quantify them. There are small scale errors with displaced ridges and headwalls, but also big parts of the images tilted. After using multiple processing setups and methods not a single attempt

was successful in creating two or more error free DTMs for a study site. It also has to be said that the current data does not have much temporal overlap. Most of the area was just researched once. For the researched study sites with data acquisition on multiple dates, the flight pattern was not optimal.

At some other areas the flight path was more lattice-like. Probably the DTM results would be better there, but differencing could not be done, because the areas were just covered once. The created workflow for creating the DTM could be applied to some of these areas to check whether the result is sufficient or not. This could be worth a try, but at the present state the outcome is not good enough.

Whether or not the heavy rain event of June/July 2021 influences the thaw slumping processes can not be said with the results of the MACS imagery. The rain falls are probably a trigger for initiating and reactivating thaw slumps. If the thawing rates in the following months or years are changing, using satellite remote sensing is a purposeful way for detecting this. But Runge et al. (2022) as well as (Lewkowicz and Way, 2019) did not find a significant link between summer rainfall amounts and RTS initiation yet. As expected, seasonal rainfalls, which they tried to link, have a different input to erosion than single extreme rainfall events do. In Summer 2021 both occurred.

After all, the DTMs are just an additional output of the flight campaigns. The main goals are large multispectral ortho mosaics, which are used for researching fire scars, ice wedge degradation, lake drainages, changing hydrology, coastal erosion and vulnerable infrastructure. Therefore MACS data acquisition will be continued anyway and also time series are just as necessary for changing detection using ortho mosaics. At the moment the DTMs can just be used for getting an 3D-overview, but if the motivation for further attempts due to new findings in progressing such data is there, also more data which can be used will be available.

5. Conclusion

The aim of this study was to find out if the airborne MACS stereo imagery can be used for quantifying coastal erosion and retrogressive thaw slumping by creating digital elevations models with a structure-to-motion attempt and differencing them. A further

goal was to determine the influence of a heavy precipitation event on the erosion, which took place on the Baldwin Peninsula in June and July 2021. The presented methods using PIX4D and QGIS were applied at two study sites. The outcome was that the DTM differencing results show some realistic elevation changes, but also have a lot of errors, which are either in the original data or occur due to processing failures. The several described errors can be found in nearly every DTM of the study sites and concern both large areas and small features. The study shows that the developed workflow for creating DTMs from the airborne MACS imagery is not successful and the data therefore can not be used for DTM differencing and detecting thermo-erosion rates and retrogressive thaw slumping. Also, it can not be researched how the heavy rainfall event, which occurred between the acquisition dates in June and July 2021, influenced the RTS. To find out about this further research has to be done. This probably works best with constant satellite data although the resolution is not as high, but the errors are less and continuous time series can be done. The MACS data DTMs can be used for getting an 3D overview of the landscape and the dynamics in general.

6. Bibliography

- Alaska Center for Climate Assessment & Policy, University of Alaska Fairbanks, funded by the NOAA Climate Program Office, 2022a. Record Rainfall in Kotzebue.
- Alaska Center for Climate Assessment & Policy, University of Alaska Fairbanks, funded by the NOAA Climate Program Office, 2022b. Record High Precipitation at Kotzebue.
- Antonova, S., Sudhaus, H., Strozzi, T., Zwieback, S., Kääh, A., Heim, B., Langer, M., Bornemann, N., Boike, J., 2018. Thaw Subsidence of a Yedoma Landscape in Northern Siberia, Measured In Situ and Estimated from TerraSAR-X Interferometry. *Remote Sens.* 10. <https://doi.org/10.3390/rs10040494>
- Berger, K., Verrelst, J., Féret, J.-B., Hank, T., Woher, M., Mauser, W., Camps-Valls, G., 2020. Retrieval of aboveground crop nitrogen content with a hybrid machine learning method. *Int. J. Appl. Earth Obs. Geoinformation* 92, 102174. <https://doi.org/10.1016/j.jag.2020.102174>
- Bergstedt, H., Jones, B.M., Hinkel, K., Farquharson, L., Gaglioti, B.V., Parsekian, A.D., Kanevskiy, M., Ohara, N., Breen, A.L., Rangel, R.C., Grosse, G., Nitze, I., 2021. Remote Sensing-Based Statistical Approach for Defining Drained Lake Basins in a Continuous Permafrost Region, North Slope of Alaska. *Remote Sens.* 13. <https://doi.org/10.3390/rs13132539>
- Berninger, A., Lohberger, S., Zhang, Siegert, F., 2019. Canopy Height and Above-Ground Biomass Retrieval in Tropical Forests Using Multi-Pass X- and C-Band Pol-InSAR Data. *Remote Sens.* 11, 2105. <https://doi.org/10.3390/rs11182105>
- Biskaborn, B.K., Smith, S.L., Noetzli, J., Matthes, H., Vieira, G., Streletskiy, D.A., Schoeneich, P., Romanovsky, V.E., Lewkowicz, A.G., Abramov, A., Allard, M., Boike, J., Cable, W.L., Christiansen, H.H., Delaloye, R., Diekmann, B., Drozdov, D., Etzelmüller, B., Grosse, G., Guglielmin, M., Ingeman-Nielsen, T., Isaksen, K., Ishikawa, M., Johansson, M., Johannsson, H., Joo, A., Kaverin, D., Kholodov, A., Konstantinov, P., Kröger, T., Lambiel, C., Lanckman, J.-P., Luo, D., Malkova, G., Meiklejohn, I., Moskalenko, N., Oliva, M., Phillips, M., Ramos, M., Sannel, A.B.K., Sergeev, D., Seybold, C., Skryabin, P., Vasiliev, A., Wu, Q., Yoshikawa, K., Zheleznyak, M., Lantuit, H., 2019. Permafrost is warming at a global scale. *Nat. Commun.* 10, 264–264. <https://doi.org/10.1038/s41467-018-08240-4>
- Brooker, A., Fraser, R.H., Olthof, I., Kokelj, S.V., Lacelle, D., 2014. Mapping the Activity and Evolution of Retrogressive Thaw Slumps by Tasselled Cap Trend Analysis of a Landsat Satellite Image Stack. *Permafr. Periglac. Process.* 25, 243–256. <https://doi.org/10.1002/ppp.1819>
- Clarke, E.S., 2007. Permafrost foundations : state of the practice, Books. American Society of Civil Engineers. <https://doi.org/10.1061/9780784409473>
- Ford, J.D., Smit, B., 2004. A Framework for Assessing the Vulnerability of Communities in the Canadian Arctic to Risks Associated with Climate Change. *Arctic* 57, 389–400.
- Hawkins, S.P., 2016. Using a drone and photogrammetry software to create orthomosaic images and 3D models of aircraft accident sites. Presented at the ISASI 2016 Seminar, Reykjavik, Iceland.
- Heim, B., Abramova, E., Doerffer, R., Günther, F., Hoesemann, J., Kraberg, A., Lantuit, H., Loginova, A., Martynov, F., Overduin, P., Wegener, C., 2014. Ocean colour remote sensing in the southern Laptev Sea: evaluation and applications. *Biogeosciences* 11, 4191–4210. <https://doi.org/10.5194/bg-11-4191-2014>
- Heuer, C.E., 1979. The Application of Heat Pipes on the Trans-Alaska Pipeline.
- Jones, B., Grosse, G., Arp, C., Jones, M., Walter Anthony, K., Romanovsky, V., 2011.

- Modern Thermokarst Lake Dynamics in the Continuous Permafrost Zone, Northern Seward Peninsula, Alaska. *J. Geophys. Res. Biogeosciences* 116, G00M03. <https://doi.org/10.1029/2011jg001666>
- Jones, B., Kolden, C., Jandt, R., Abatzoglou, J., Urban, F., Arp, C., 2009. Fire Behavior, Weather, and Burn Severity of the 2007 Anaktuvuk River Tundra Fire, North Slope, Alaska. *Arct. Antarct. Alp. Res.* 41, 309–316. <https://doi.org/10.1657/1938-4246-41.3.309>
- Jones, B.M., Breen, A.L., Gaglioti, B.V., Mann, D.H., Rocha, A.V., Grosse, G., Arp, C.D., Kunz, M.L., Walker, D.A., 2013. Identification of unrecognized tundra fire events on the north slope of Alaska. *J. Geophys. Res. Biogeosciences* 118, 1334–1344. <https://doi.org/10.1002/jgrg.20113>
- Jongejans, L., Strauss, J., Lenz, J., Peterse, F., Mangelsdorf, K., Fuchs, M., Grosse, G., 2018. Organic matter characteristics in yedoma and thermokarst deposits on Baldwin Peninsula, west Alaska. *Biogeosciences* 15, 6033–6048. <https://doi.org/10.5194/bg-15-6033-2018>
- Jorgenson, J., Jorgenson, M., Boldenow, M., Orndahl, K., 2018. Landscape Change Detected over a Half Century in the Arctic National Wildlife Refuge Using High-Resolution Aerial Imagery. *Remote Sens.* 10, 1305. <https://doi.org/10.3390/rs10081305>
- Jorgenson, M., Yoshikawa, K., Kanevskiy, M., Shur, Y., Romanovsky, V., Marchenko, S., Grosse, G., Brown, J., Jones, B., 2008. Permafrost characteristics of Alaska, Proceedings of the Ninth International Conference on Permafrost.
- Jorgenson, M.T., Brown, J., 2005. Classification of the Alaskan Beaufort Sea Coast and estimation of carbon and sediment inputs from coastal erosion. *Geo-Mar. Lett.* 25, 69–80. <https://doi.org/10.1007/s00367-004-0188-8>
- Kasischke, E., Turetsky, M., Kane, E., 2012. Effects of trees on the burning of organic layers on permafrost terrain. *For. Ecol. Manag.* 267, 127–133. <https://doi.org/10.1016/j.foreco.2011.12.009>
- Klein, K.P., Lantuit, H., Heim, B., Doxaran, D., Juhls, B., Nitze, I., Walch, D., Poste, A., Søreide, J.E., 2021. The Arctic Nearshore Turbidity Algorithm (ANTA) - A multi sensor turbidity algorithm for Arctic nearshore environments. *Sci. Remote Sens.* 4, 100036. <https://doi.org/10.1016/j.srs.2021.100036>
- Lantuit, H., Pollard, W., 2005. Temporal stereophotogrammetric analysis of retrogressive thaw slumps on Herschel Island, Yukon Territory. *Nat. Hazards Earth Syst. Sci.* 5. <https://doi.org/10.5194/nhess-5-413-2005>
- Lewkowicz, A.G., Way, R.G., 2019. Extremes of summer climate trigger thousands of thermokarst landslides in a High Arctic environment. *Nat. Commun.* 10, 1329. <https://doi.org/10.1038/s41467-019-09314-7>
- Ling, F., Zhang, T., 2003. Impact of the timing and duration of seasonal snow cover on the active layer and permafrost in the Alaskan Arctic. *Permafr. Periglac. Process.* 14, 141–150. <https://doi.org/10.1002/ppp.445>
- Marzen, M., Iserloh, T., Lima, J.L.M.P. de, Fister, W., Ries, J.B., 2017. Impact of severe rain storms on soil erosion: Experimental evaluation of wind-driven rain and its implications for natural hazard management. *Sci. Total Environ.* 590–591, 502–513.
- Necsoiu, M., Dinwiddie, C., Walter, G., Larsen, A., Stothoff, S., 2013. Multi-temporal image analysis of historical aerial photographs and recent satellite imagery reveals evolution of water body surface area and polygonal terrain morphology in Kobuk Valley National Park, Alaska. *Environ. Res. Lett.* 8. <https://doi.org/10.1088/1748-9326/8/2/025007>
- Nitze, I., Cooley, S., Duguay, C., Jones, B., Grosse, G., 2020. The catastrophic thermokarst

- lake drainage events of 2018 in northwestern Alaska: Fast-forward into the future. *The Cryosphere* 14, 4279–4297. <https://doi.org/10.5194/tc-14-4279-2020>
- Nitze, I., Rettelbach, T., 2021. Prepare_MACS_Processing.ipynb.
- Obu, J., 2021. How Much of the Earth's Surface is Underlain by Permafrost? *J. Geophys. Res. Earth Surf.* 126, e2021JF006123. <https://doi.org/10.1029/2021JF006123>
- Obu, J., Lantuit, H., Fritz, M., Pollard, W., Sachs, T., Günther, F., 2016. Relation between planimetric and volumetric measurements of permafrost coast erosion: A case study from Herschel Island, western Canadian Arctic. *Polar Res.* 35, 30313. <https://doi.org/10.3402/polar.v35.30313>
- Obu, J., Lantuit, H., Grosse, G., Günther, F., Sachs, T., Helm, V., Fritz, M., 2017. Coastal erosion and mass wasting along the Canadian Beaufort Sea based on annual airborne LiDAR elevation data. *Permafr. Periglac. Res. Coasts Mt.* 293, 331–346. <https://doi.org/10.1016/j.geomorph.2016.02.014>
- Paine, J., Andrews, J., Saylam, K., Tremblay, T., Averett, A., Caudle, T., Meyer, T., Young, M., 2013. Airborne LiDAR on the Alaskan North Slope: wetlands mapping, lake volumes, and permafrost features, *The Leading Edge*. <https://doi.org/10.1190/segam2013-1488.1>
- Paltan, H., Dash, J., Edwards, M., 2015. A refined mapping of Arctic lakes using Landsat imagery. *Int. J. Remote Sens.* 36, 5970–5982. <https://doi.org/10.1080/01431161.2015.1110263>
- Porter, C., Morin, P., Howat, I., Noh, M.-J., Bates, B., Peterman, K., Keeseey, S., Schlenk, M., Gardiner, J., Tomko, K., Willis, M., Kelleher, C., Cloutier, M., Husby, E., Foga, S., Nakamura, H., Platson, M., Wethington, M., Jr., Williamson, C., Bauer, G., Enos, J., Arnold, G., Kramer, W., Becker, P., Doshi, A., D'Souza, C., Cummins, P., Laurier, F., Bojesen, M., 2018. ArcticDEM. <https://doi.org/10.7910/DVN/OHHUKH>
- Poujol, B., Prein, A., Newman, A., 2020. Kilometer-scale modeling projects a tripling of Alaskan convective storms in future climate. *Clim. Dyn.* 55. <https://doi.org/10.1007/s00382-020-05466-1>
- Rettelbach, T., Langer, M., Nitze, I., Jones, B., Helm, V., Freytag, J.-C., Grosse, G., 2021. A Quantitative Graph-Based Approach to Monitoring Ice-Wedge Trough Dynamics in Polygonal Permafrost Landscapes. *Remote Sens.* 13, 3098. <https://doi.org/10.3390/rs13163098>
- Runge, A., Nitze, I., Grosse, G., 2022. Remote sensing annual dynamics of rapid permafrost thaw disturbances with LandTrendr. *Remote Sens. Environ.* 268, 112752. <https://doi.org/10.1016/j.rse.2021.112752>
- Ruzgiene, B., 2014. Analysis of camera orientation variation in airborne photogrammetry: images under tilt (roll-pitch-yaw) angles. *J. Meas. Eng.* 2, 95–102.
- Scheffler, D., Hollstein, A., Diedrich, H., Segl, K., Hostert, P., 2017. AROSICS: An Automated and Robust Open-Source Image Co-Registration Software for Multi-Sensor Satellite Data. *Remote Sens.* 9. <https://doi.org/10.3390/rs9070676>
- Schuur, T., 2019. Permafrost and the Global Carbon Cycle. *Arct. Rep. Card* 2019.
- Shaw, J.M., Taylor, R.B., Solomon, S.M., Christian, H.A., Forbes, D.L., 1998. Potential impacts of sea level rise of Canadian coasts. *Can. Geogr.* 42.
- Stettner, S., Lantuit, H., Heim, B., Eppler, J., Roth, A., Bartsch, A., Rabus, B., 2018. TerraSAR-X Time Series Fill a Gap in Spaceborne Snowmelt Monitoring of Small Arctic Catchments—A Case Study on Qikiqtaruk (Herschel Island), Canada. *Remote Sens.* 10, 1155. <https://doi.org/10.3390/rs10071155>
- Sweeney, C., 2016. Theia Multiview Geometry Library: Tutorial & Reference.
- Turetsky, M.R., Abbott, B.W., Jones, M.C., Anthony, K.W., Olefeldt, D., Schuur, E.A.G., Grosse, G., Kuhry, P., Hugelius, G., Koven, C., Lawrence, D.M., Gibson, C.,

- Sannel, A.B.K., McGuire, A.D., 2020. Carbon release through abrupt permafrost thaw. *Nat. Geosci.* 13, 138–143. <https://doi.org/10.1038/s41561-019-0526-0>
- Ulrich, M., Grosse, G., Strauss, J., Schirrmeister, L., 2014. Quantifying Wedge-Ice Volumes in Yedoma and Thermokarst Basin Deposits. *Permafr. Periglac. Process.* 25, 151–161. <https://doi.org/10.1002/ppp.1810>
- Van der Sluijs, J., Kokelj, S.V., Fraser, R.H., Tunnicliffe, J., Lacelle, D., 2018. Permafrost Terrain Dynamics and Infrastructure Impacts Revealed by UAV Photogrammetry and Thermal Imaging. *Remote Sens.* 10. <https://doi.org/10.3390/rs10111734>
- Van Everdingen, R., 2005. Multi-language glossary of permafrost and related ground-ice terms. *Natl. Snow Ice Data Centerworld Data Cent. Glaciol.*
- Wendler, G., Gordon, T., Stuefer, M., 2017. On the Precipitation and Precipitation Change in Alaska. *Atmosphere* 8, 253. <https://doi.org/10.3390/atmos8120253>
- Young, A.P., Guza, R.T., Matsumoto, H., Merrifield, M.A., O'Reilly, W.C., Swirad, Z.M., 2021. Three years of weekly observations of coastal cliff erosion by waves and rainfall. *Geomorphology* 375, 107545. <https://doi.org/10.1016/j.geomorph.2020.107545>

Eidesstattliche Erklärung

Hiermit versichere ich, dass ich die vorliegende Arbeit selbstständig verfasst und keine anderen als die angegebenen Quellen und Hilfsmittel benutzt habe, alle Ausführungen, die anderen Schriften wörtlich oder sinngemäß entnommen wurden, kenntlich gemacht sind und die Arbeit in gleicher oder ähnlicher Fassung noch nicht Bestandteil einer Studien- oder Prüfungsleistung war.

München, den 01.02.2022

Simon Schäffler

Ort, Datum